Science of the Total Environment 965 (2025) 178650

Contents lists available at ScienceDirect

Science of the Total Environment

journal homepage: www.elsevier.com/locate/scitotenv

Pyrolytic conversion of construction, renovation, and demolition (CRD) wood wastes in Québec to biochar: Production, characterization, and identifying relevant stability indices for carbon sequestration

Aravind Ganesan *, Olivier Rezazgui, Simon Langlois, Cyrine Boussabbeh, Simon Barnabé

Université du Québec à Trois-Rivières Trois-Rivieres, Quebec, Canada

HIGHLIGHTS

- Québec contributes to 13 % of overall CRD wood waste generation in Canada
- Slow pyrolysis was chosen to valorize non-recyclable CRD wood waste to bioproducts
- Horizontal tube furnace carbonized CRD wood with good physiochemical properties
- Pyrolysis temperature significantly influenced biochar properties (p-value ≤ 0.05)
- Raman I_D/I_G, H/C, O/C, and proximate analysis are reliable stability indices

GRAPHICAL ABSTRACT

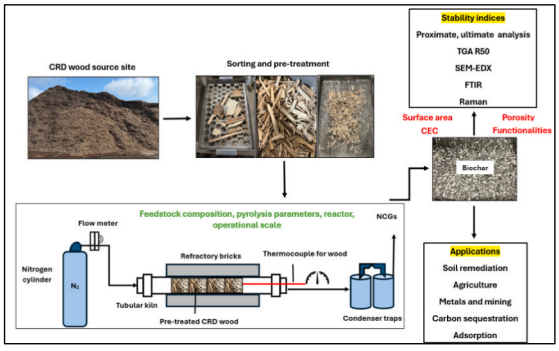

ARTICLE INFO

Editor: Elena Paoletti

Keywords:
CRD
Biochar
Stability
Pyrolysis
Biomass
Aromatic
Thermochemical

ABSTRACT

Management of heterogeneous construction, renovation, and demolition (CRD) wood residues in Québec brings into light, a widespread topic under discussion related to their current disposal methods in landfills, that may lead to environmental concerns. With rising forfeitures from a legal standpoint, alternative treatment methods for CRD wood wastes are being explored. Thermochemical biomass conversion techniques can be employed to depolymerize low-quality end-of-life CRD wood and valorize it to bio-based products. Biochar, a carbonaceous material obtained through heat treatment of wood under the absence of oxygen *via* slow pyrolysis, can be tailored for specific end-use applications in hard-to-abate industrial sectors pertinent to energy, composite materials, and environmental amendments. However, there is a scarcity of comprehensively understanding CRD wood pyrolysis and projecting the biochar product's stability due to a lack of relevant studies and frequent inconsistencies amidst currently available methods. Nevertheless, in the present study, CRD wood is pyrolyzed in a horizontal tube furnace of two scales under laboratory conditions. Temperatures ranging from 300 to 800 °C, biomass residence time (BRT) of 30–120 min, heating rates of 20–55 °C/min, and mass of feedstock between 100 and 500 g were the operational conditions chosen for experimentation. Evaluation of biochar stability was carried out by the proximate and ultimate analysis, Van-Krevelen plots, TGA/DTG profile, R50 recalcitrance, SEM-EDX, and Raman I_D/I_G methods. Data analysis indicated that carbon content (89–90 %), FC (70–74 %), TSF (73–75 %), R50 (0.64–0.65), and I_D/I_G (0.972) increased with an increase in BRT (120 min) and pyrolysis

* Corresponding author.
E-mail address: Aravind.Ganesan@uqtr.ca (A. Ganesan).

https://doi.org/10.1016/j.scitotenv.2025.178650
Received 3 December 2024; Received in revised form 23 January 2025; Accepted 24 January 2025
Available online 29 January 2025

temperature (800 °C) rendering its utilization in metallurgical applications as a reductant. A surface area of 220–270 m^2/g was also detected for these biochar at 800 °C recommending its implementation for adsorption applications. Biochar's cation exchange capacity (CEC), pH, and hydrophobicity also increased at high temperatures nurturing the ability to be used for soil pH adjustment as part of remediation activities. SEM-EDX proved that ash content predominantly harboring alkaline and alkaline earth metals (AAEM) like Ca and K also increased but to a certain point from where their devolatilization is implicit, thereby concentrating stable carbon. As for functionalities in biochar, they decreased from 500 to 800 °C verifying the rejection of oxychemicals groups. Noticeable striations associated to C-H/C-O/C=O vibration, stretching, and bending from FTIR spectral bands were linked to terminal dehydrogenation, condensation, and aromatization reactions highlighting the development of C—C and C=C linkages commonly assigned to aromatics. Evident from low Van-Krevelen H/C (0.51–0.09) and O/C (0.08–0.02) indices, it can be extrapolated that high-temperature biochars in PR:1 and PR:2 possess a high permeance that could bolster its utilization in carbon sequestration/draw-down and other CDR applications.

Nomenclature

AAEM	Alkaline and alkaline earth metals
ANZBIG	Australia NewZealand biochar industry group
ANOVA	Analysis of variance
BET	Brunauer-Emmett-Teller
BRT	Biomass residence time
CEC	Cation exchange capacity
CHP	Combined heat and power
CDR	Carbon dioxide removal
CRD	Construction renovation and demolition
DB	Dry basis
DTG	Differential thermogram
DMW	Demineralized water
EAF	Electric arc furnace
EBI	European biochar industry
EDX	Energy dispersive spectroscopy
FC	Fixed carbon
FTIR	Fourier transform infrared
HTL	Hydrothermal liquefaction
HTT	Heat treatment temperature
IBI	International biochar initiative
ICI	Institutional commercial and industrial
MAH	Monoaromatic hydrocarbon
MP-AES	Microwave plasma atomic emission spectrometer
NCG	Non-condensible gas
NMR	Nuclear magnetic resonance
PAH	Polyaromatic hydrocarbon
PR:1	Pyrolysis round 1
PR:2	Pyrolysis round 2
R&R	Repeatability and reproducibility
SEM	Scanning electron microscope
SPT	Setpoint temperature
TGA	Thermogravimetric analysis
TSF	Thermostable fraction
VC	Volatile carbon
VM	Volatile matter
VOC	Volatile organic compound
XRD	X-ray diffraction

1. Introduction

The Québec Ministry of Forests, Wildlife, and Parks has prioritized sustainable construction practices through policies like the Wood Charter which promotes the use of responsibly sourced timber in residential, industrial, and commercial sectors. Québec's forests, rich in hardwood and softwood species, support eco-friendly building initiatives while generating economic benefits such as job creation, R&D, investments, and trade, all contributing to climate change mitigation. CRD waste management remains a challenge, with Québec producing 1.85 Mt. annually, including 56 % wood alongside metals, plastics, and other materials (Recyc-Québec, *2018*). Of this, 1.67 Mt. ends up in landfills, including significant contributions from municipal, industrial, and commercial sectors (Recyc-Québec, *2021*). Though 53 % of CRD wood waste is recovered for alternative uses, 63 % among this is diverted for energy recovery and 37 % is repurposed for products like furniture and panels (Recyc-Québec, *2018*).

This work focuses exclusively on CRD wood sourced from Québec, emphasizing the environmental and economic benefits of recycling locally available wood waste. CRD wood recycling faces hurdles such as issues related to wear/damage and economic constraints with recovery costs ranging from $31.6/t to $181/t depending on quality (Schorr and Boivin, *2023*). CRD wood recycling in the province is also hindered by contamination from chemicals (*e.g.*, arsenic, chromium, copper, creosote, and lead) in treated and painted wood, variability in wood composition, and logistical barriers. Treated wood poses environmental risks, releasing these heavy metals, chemicals, and VOCs during disposal if not managed properly. Since Québec contributes to 13 % of Canada's CRD wood waste with over 50 % comprising of such treated wood, emphasizing the importance of localized valorization is necessary (Schorr and Boivin, *2023*). Provincial legislations such as "Q2, r.19 – landfill and incineration" monitor the handling of hazardous CRD materials. Components like gypsum in drywalls release harmful gases (*e.g.*, H_2S) upon landfill disposal, exacerbating environmental penalties. Stricter legal mandates coupled with stakeholder collaboration and policy incentives necessitate alternative treatment methods for heavily contaminated CRD wood management.

Owing to certain difficulties in the recycling and landfilling spheres, CRD wood waste to energy conversion could be an approach that is well-sought-after. Firstly, being a renewable source, it can be replenished *via* the highly -appreciated sustainable forestry practices in Québec like preventing illegal logging, regeneration and harvesting, reforestation, and agroforestry. Secondly, since it is biomass, it is considered carbon-neutral because the CO_2 released from its energetic valorization is re-captured by trees during their lifecycle. Thirdly, since CRD wood wastes will be diversely available in future because of enhanced utilization in construction within the province, there could be a steady source of supply. Fourthly, utilizing CRD wood fosters local energy security and reduces the reliance on imports. Next, it promotes a genuinely healthy image of waste reduction *via* a circular economy principle that minimizes landfill treatment and ecological/societal concerns. Finally, the province's abundant natural resources, historical use of wood in construction, and industrial landscape—home to leading metal and

alloy producers in the world—test the use of non-recyclable, contaminated CRD wood nowadays as an engineered metallurgical-grade energy source to replace fossil coal or coke. Regional demands promoting carbon sequestration and climate resilience further strengthen the potential for utilizing bioproducts derived from locally sourced CRD wood waste in other applications like soil remediation, horticulture, and agriculture.

Heat aids in faster depolymerization of wood wastes and produces a gamut of products in the solid, liquid, and gaseous forms that can find many attributes. Pyrolysis is an effective thermochemical treatment for the valorization of wood waste at increasing temperatures with limited intervention of air or oxygen to bioproducts of added value like biochar, pyrolysis gas, and biooil (Tian et al., 2020). It can be streamlined into either slow, fast or flash pyrolysis corresponding to the employed pyrolysis temperature, heating rate, and BRT (Panwar, *2024*). Slow pyrolysis is distinguished by a low pyrolysis temperature, long BRT, and slow heating rate that favours solid biochar yield. An intermediate or moderate pyrolysis temperature, short BRT, and high heating rate maximizes liquid biooil yield *via* fast pyrolysis. Whereas an exceedingly high pyrolysis temperature, noticeably short BRT, and very high heating rate indicate flash pyrolysis that enhances gas yield (Hasan et al., 2022).

As delineated in Supplementary figure 1, CRD wood pyrolysis can be bifurcated into two types: primary and secondary pyrolysis (Muema et al., 2024). During primary pyrolysis, the hemicellulose, cellulose, and lignin polymers in biomass breakdown in an order, to produce steam (surface and loosely bound water), light gases, primary condensable volatiles (biooil), and primary biochar composed of mono-aromatic rings that begin to confer its stability (Yang et al., 2021). The onset of secondary heterogeneous pyrolysis reactions is kicked off at higher temperatures where in-bound/interstitial water molecules are volatilised to form secondary steam, followed by cracking of more unstable/low-molecular weight volatiles that induces the formation of condensed secondary biooil along with secondary char entailing poly-aromatic rings. *i.e*, 2 or more benzene rings attached (Dieguez-Alonso et al., 2015). Cracking is also mainly insinuated by primary condensed volatiles settled on biomass and primary biochar, when exposed to prolonged heated atmospheres without being entrained from the reactor (Dieguez-Alonso et al., 2015). Extrapolating a finding from Fawaz et al., 2021, a major drawback associated to secondary pyrolysis through such cracking reactions is that it could yield low carbon conversion in biochar and biooil due to significant loss of carbon in secondary pyrolysis gases (including CO, CO_2, CH_4, and other C_1-C_3 gases).

Biochar is a carbon rich substance that characterized by its porous, honeycomb-like framework with appreciable physico-chemical properties for use in agriculture, construction, and metallurgical sectors (*Bindar et al., 2024a, b*). Biooil is the liquid, organic product fraction that is rich in a myriad of chemical compounds including but not limited to alcohols, acids, aldehydes, ketones, and aromatics (Steven et al., 2024). The biooil can be further refined to optimize its physical and chemical properties for the production of chemicals and fuels (resembling gasoline, diesel, jet fuel, or marine fuel) or can be burnt directly in boilers or furnaces for energy generation. It can also be used to produce distillate fractions serving as precursors for sustainable chemicals (Oktavia et al., 2024). Pyrolysis gas consists of components such as CO, CO_2, CH_4, CO_2, SO_X, and NO_X (Kasmiarno et al., 2024). Pyrolysis gas can either be combusted to produce heat/electricity in a combined heat and power (CHP) plant, can be looped back to supply a part of the energy for pyrolysis, or can be a foundation for the production of synfuels. Relative to other thermochemical treatments like hydrothermal liquefaction (HTL), gasification or combustion, pyrolysis offers a multitude of product stream with appreciable yields, can be optimized, does not require: air, water or oxygen, specialized gas cleaning/upgrading equipment, high temperature or catalyst (Dada et al., 2021).

Ideally, CRD wood wastes like furniture wood, plywood, panels, and particle boards could be converted to biofuels or bioproducts through slow or fast pyrolysis (Kim et al., 2014). Some articles highlight the production of biooil from CRD wood material through fast pyrolysis in batch and fluidized bed reactors where a moderate temperature of 400–550 °C can produce yields ranging from 30 to 60 wt% (Heo et al., 2010; Jung et al., 2012; Kim et al., 2014). Higher temperatures with low BRT produced more gases particularly comprising of CO, CO_2, H_2, H_2S, SO_x, NO_X, and C_1-C_3 gases. Whereas lower temperatures and higher BRT produced more biochar with yields ranging from 30 to 35 wt%.

In recent time, biochar is being researched as a promising carbon dioxide removal (CDR) tool by virtue of its thermostability, high carbon pool locked in, and partly recalcitrant nature in natural surroundings. On grounds of its ideal micro to *meso* porosity, surface functional groups, surface area and pore volume, biochar is being investigated for multi-disciplinary end-uses like soil fertility improvement, substitute for peat in plant growth media, adsorbent material in feed for rumen animals, wastewater treatment, coloring agent for automotive parts, and construction materials. CRD wood wastes can be pyrolyzed under a myriad of process parameters including but not limited to treatment temperature, BRT, heating rate, and/or mass of feedstock processed. These conditions mainly, can be optimized to produce biochar of appreciable quality and yield, with respect to the intended application under focus. For example, in metallurgical processes involving high temperatures and pressures, pyrolytic biochar could partially substitute coal, coke or anthracite in the blast or electric arc furnace (EAF) as an effective chemical reductant without adverse degradation provided it has a high carbon content, low oxygen, low moisture and ash, high stability, heat conductivity, heating value, and minimal to moderate surface area (well-distributed pore network) (Ye et al., 2019). These properties of biochar can also support the slag interaction and metal ore melting processes. Whereas, for areas concerning pollutant gas adsorption or treating wastewater, with high surface area and porosity probably being supportive, a very high carbon (>90 %) is not a pre-requisite.

The focus on locally sourced CRD wood ensures relevance to Québec's specific environmental, economic, and industrial contexts, reinforcing the province's leadership in sustainable wood recycling and biochar production. This concentrated approach enhances the feasibility of integrating biochar into Québec's sustainability efforts while addressing the region's unique challenges and opportunities. To the best of our knowledge, there has not been a study on the pyrolytic valorization of CRD wood wastes in Québec to biochar with its characterization pertinent to stability and environmental permeance which is viewed as a major research gap.

Using this knowledge gap as a foundation, the following hypotheses are outlined sequentially: 1) mechanical methods of CRD waste separation to wood and inorganic fractions will eliminate the influence of minerals and metal components during pyrolysis. Additionally, size separation of the wood fraction tapers the optimal particle size for pyrolysis; 2) mild acid washing of milled CRD wood (as chips) will leach higher AAEM concentrations; 3) horizontal tube furnace facilitates efficient conversion of pre-treated CRD wood chips due to better heat management and lower thermal inertia; 4) pyrolysis under a range of different temperatures, BRT, and/or heating rate can greatly influence the properties of biochar circumventing physical and chemical stability.

Therefore, in the present article, we will be covering the following objectives: a) importance of CRD wood sorting and chemical pre-treatment to leach labile AAEM and other soluble metals; b) testing two types of horizontal tube reactors with augmented process design to produce biochar; c) characterization of CRD biochars and analyzing the role of pyrolysis parameters, biomass composition on its properties; and d) establishing some “potential” stability indices for biochar-based carbon sequestration and other applications.

As deliverables, firstly, various biochar stability assessment methods and their respective categories, which will be leveraged to address the core aim of the study, will be shortlisted. A brief description of each method will then be provided along with an explanation of the mathematical equations/formulae to be utilized. Following this, CRD biomass size separation, contaminant removal, milling, and characterizations will take place. Pyrolysis of biomass using a laboratory small-scale

horizontal tubular furnace reactor and a scaled-up tubular furnace reactor will proceed, followed by the characterization of the resulting biochars to analyze the effect of feedstock composition, pyrolysis conditions, and process optimization on their physiochemical and structural properties. Finally, the most reliable parameters for indexing biochar stability along with potential applications will be discussed.

2. Materials and methods

Prominent methods to quantify biochar stability into three classes is discussed here prior to deciding the characterizations to be performed.

2.1. Biochar stability - theory

Despite its potential in climate change mitigation, assessing biochar's stability remains complex, necessitating improved evaluation techniques. Biochar's permeance is not as permanent as minerals and strongly depends on its carbon ring structures, which are formed through rapid chemical transformations during pyrolysis (*Chiaramonti et al., 2024a, b*; Adhikari et al., 2024). Stability indices are categorized into three domains. Firstly, alpha indices like Van-Krevelen parameters (H/C and O/C) are widely used, cost-effective indicators of biochar's aromatic condensation and environmental resistance (Budai et al., 2013). Proximate analysis, assessing fixed carbon (FC), volatile carbon (VC), and ash content, also aids in understanding stability (Spokas, *2010*). Other methods of correlation to study biochar's permeance as a carbon sink are still being optimized mainly due to biochar's heterogeneous carbon pools that are not uniformly represented (*Klasson, 2017*). These beta methods include incubation experiments, involving chemical aging with oxidizing agents (eg: H_2O_2, $KMnO_4$) evaluate biochar's oxidation behaviour and mean residence time in soil but are labour-intensive and time-consuming (Cross and Sohi, *2013*) procedures. Finally, gamma indices harboring instrumental techniques like ^{13}C NMR, FTIR, Raman spectroscopy, and XRD analyze biochar's structural properties including aromaticity and crystalline composition to infer durability (Wood et al., 2024).

Although these methods provide valuable insights, they require rigorous updates to account for environmental variables such as soil acidity, alkalinity, and composition, especially when biochar is used in agriculture or soil-based CDR applications.

2.1.1. Other metrics for biochar stability

Aside from renowned conventional metrics, two other stability indices were adopted in an attempt to evaluate the biochars produced from in-house pyrolysis experiments.

2.1.1.1. Thermostable fraction (TSF): Category 1 or alpha. TSF is represented through the ratio of FC to the cumulative value of VC and FC derived from proximate analysis of biochar. Eq. 1 is adapted from Adhikari et al., 2024 to replace VC in place of VM since the biochar sample is already pre-dried to eliminate as much moisture as possible.

$$\text{TSF}\ (\%) = \left(\frac{\text{FC}}{\text{VC} + \text{FC}}\right) \times 100 \tag{1}$$

2.1.1.2. TGA R50: Category 2 or beta. Oxidation resistance of biochar was calculated using a low-cost assessment *via* thermogravimetric analysis (TGA) and by incorporating an index of recalcitrance called R50 (Yang et al., 2018). It is a quantitative screening tool to predict biochar's mineralization tendency. A higher R50 value is an indication for greater stability and recalcitrance (Li and Chen, *2018*). Pyrolysis parameters, mainly temperature, along with heat treatment duration, and nature of feedstock are directly proportional to this R50 value (Wang et al., 2021; Harvey et al., 2012). The aforementioned authors classify R50 values into three types: Class A (R50 $\geq$ 0.7) suggesting least biodegradation; Class B (0.5 $\leq$ R50 $<$ 7) with moderate degradation; and Class C (R50 $<$ 0.5), showing highest susceptibility to degradation. From the raw thermogram, R50 is calculated using Eq. 2:

$$\text{R50} = \left(\frac{T_{50\%\text{weight loss for biochar}}}{T_{50\%\text{weight loss for graphite}}}\right) \tag{2}$$

Here, $T_{50\%\ \text{weight loss for biochar}}$ was the temperature in °C obtained from the raw thermogram of a biochar sample where it experienced exactly 50 % of its weight loss. Likewise, $T_{50\%\ \text{weight loss for graphite}}$ was the theoretical temperature in °C obtained for 50 % weight loss of a reference graphite material. Different values for $T_{50\%\ \text{weight loss for graphite}}$ were used such as 844 °C in Wang et al., 2021 and 886 °C as in Chen et al., 2021. In this article, 886 °C was used for calculating the R50 value because it is more common amidst literatures that try to compute biochar carbon stability using this method. However, before the respective temperatures where 50 % weight loss of biochar were recorded, the thermograms were first corrected for moisture and ash content using the method discussed in Harvey et al., 2012. This ensures that the weight loss was only occurring in the carbonaceous fraction of biochar. To correct the thermogram, Eq.3 is used:

$$W_{i,\text{corrected}} = 100 + \left[100 \times \left[\frac{W_{i,\text{uncorrected}} - W_{200,\text{ucorrected}}}{W_{200,\text{uncorrected}} - W_{\text{cutoff,uncorrected}}}\right]\right] \tag{3}$$

Here, $W_{i,\text{corrected}}$ was the final corrected weight of biochar in the thermogram, $W_{i,\text{uncorrected}}$ was the initial uncorrected weight of biochar sample during the initiation of the TGA process, $W_{200,\text{uncorrected}}$ was the weight of biochar at 200 °C at which free and non-structural water was believed to be lost or the point after which weight loss was largely attributed to organic carbon decomposition (Yaashikaa et al., 2020), and $W_{\text{cutoff,uncorrected}}$ was the final weight of biochar in the TGA process where it faced no additional oxidation or further loss of weight. All $W_{\text{uncorrected}}$ values were obtained as percentage weights of the sample at that particular temperature from the raw thermogram.

Predicting biochar stability indices still remains challenging due to inconsistencies in available methods, requiring further research to establish robust evaluation criteria. Some methods available to examine stable biochar and the methods that will be used in this work are discussed inSupplementary table1.

2.2. Biomass preparation for pyrolysis

2.2.1. Size separation

As in Fig. 1, a mix of CRD wood of varying particle sizes was sourced from “BRQ Fibre et Broyure”, Trois-Rivières, Québec, Canada (A). It was collected and brought to the Innofibre's Thermobiom premises at Trois-Rivières in buckets (B). Then, the mix was size separated (C) in a mechanically vibrated sieve of pore sizes >45 mm (E), >7 mm (F), >5 mm (G), and > 3 mm (H) with the last tray allotted for any fines. Any contaminants found in the wood mix like glass, plastic, nylon, rubber, and rocks were retrieved and segregated (D).

2.2.2. Milling

A Retsch SM300 with a 3 kW motor, coupled with a high speed tungsten carbide rotor of variable speeds of 100–3000 rpm, was used for fines generation through milling. The pore size of screens can go down to as low as 500 μm for the apparatus. This equipment was used to produce powder-like material of both, biomass and biochar for their individual characterizations.

2.3. Biochar characterization

2.3.1. Proximate analysis

For proximate analysis, the percentage of ash was quantified using a muffle furnace as per ISO 1171. Other available standards include EN 14775 or DIN 51719 (*McLaughlin, 2018*). 1 g of powdered and dry biochar was taken in an open ceramic crucible and heated at a rate of 5

Fig. 1. CRD wood sorting, size-separation, and contaminant removal.

K/min from ambient temperature to 106 °C, where it was held for 60 min. Then the temperature was ramped up to 550 °C with the same heating rate and once again, held for 120 min. Finally, the crucible was removed from the oven and cooled in a dessicator for 15–20 min before the residual weight of biochar was measured for ash determination. For VC, 1 g of powdered and dry biochar was taken in a quartz sealed quartz crucible. Once the temperature of the muffle furnace was set at 900 °C, the crucible was placed inside for exactly 7 min. Following this, the crucible was cooled down in a dessicator for 15–20 min before weighing to determine the labile carbon lost. FC was calculated by using the formula: 100-(VC + ash), on a dry basis (%DB). This formula was adopted from *Tu et al. (2022)* for VC in place of VM since our sample was already dried and moisture-deprived.

2.3.2. Ultimate analysis

To compute the percentage of elements like C, H, N, S, an Elementar Vario Macro Cube was used that has an add on Cl detector too. About 60 samples with varying sample weights of 1–200 mg can be loaded under the influence of helium (purity>99.996 %) as carrier gas. Combustion in the presence of >99.996 % oxygen till a temperature of 1200 °C can achieved with the instrumentation. With the value of ash from proximate analysis, O was calculated by difference as [100-(C + H + N + S + ash)] suggested by *Chen et al., 2022a, b*.

2.3.3. TGA

To study the variation in weight loss with temperature, a PerkinElmer TGA 8000 analyzer was used. It can also measure proximate analysis metrics like moisture, VM, and ash. About 48 samples can be processed at once with just 8 mg of powdered biochar as is (without drying) in each vial. About 1200 °C can be accurately reached with this set-up with varying heating rates. For our analysis, compressed air was preferred to study the oxidation behaviour of biomass and biochars at a heating rate of 10 °C/min till a maximum temperature of 900 °C.

2.3.4. FTIR

Agilent Technologies' Cary 630 spectroscope equipped with a Microlab PC software was used to analyze the surface functional group distribution on biochar. About 1 g of dry biochar powder, was placed on the surface of a diamond or germanium crystal after periodic cleaning with ethanol, for the determination of chemical bonds that make up the solid material, using the transmittance function with a spectral range of 1000–4000 cm^{-1}. No normalization or baseline peak correction were performed for the spectral peaks. Assigning peaks to their associated functionalities was carried out following a library as mentioned in *Johnston, 2017*.

2.3.5. Raman spectroscopy

To analyze the amorphous and highly stable/graphitic carbon make-up in powdered dry biochar, a ThermoScientific DXR3 Raman Spectroscope with a laser power of 7 mW, collection exposure time of 60 s, and a laser excitation wavelength of 532 nm for carbonaceous materials, was used. The diameter which the laser spot could cover can be as low as 1 μm that aided a wider coverage of biochar crystallites. Recorded spectra were under the wavenumber range of 800–1800 cm^{-1}. The ratio of D and G band as I_D/I_G, was used to represent the evolution of biochar's microstructure or degree of graphitization as pyrolysis temperature increased from 500 °C to 800 °C.

2.3.6. Bet

Micrometrics Tristar II with a deaerator system to remove impurities, was used to measure the specific surface area and pore volume of dry biochar powder through nitrogen or helium gas physisorption. Pore sizes varying from 0.35 to 100 nm can be detected using this instrumentation, beginning from 0.01 m^2/g.

2.3.7. Metals

For the detection of metals and other sensitive elements in dry biochar powder, Agilent Technologies' 4210 Microwave Plasma Atomic Emission Spectrometer (MP-AES) operating with nitrogen as fuel source and a SPS 4 autosampler, was used. It allows simultaneous multi-element analysis by nebulizing the biochar sample into a nitrogen plasma to form monoatomic ions. To precisely measure the inorganic content, organic matter in biochar was digested completely by the instrumentation.

2.3.8. pH

Dry biochar powder, at a 1:10 weight ratio with demineralized water (DMW), was mixed with a magnetic stirring plate for 60 min. Post shaking, a bench-top pH analyzer was used to measure the pH of the biochar suspension.

2.3.9. Bulk density of biomass

The bulk density of CRD wood to figure out the type of wood it harbored, was carried out according to a method discussed in Pahnila et al., 2024. A steel container of a known mass and volume was filled with the heterogeneous CRD wood (before size separation). The surface of the wood mix was evenly levelled to take away excess material and the mass of the container was re-weighed. With the difference in mass of container with and without the CRD wood and its known volume, the bulk density is calculated using Eq. 4:

$$\text{Bulk density}\left(\frac{\text{kg}}{\text{m3}}\right) = \frac{(\text{Mass of container with CRD biomass} - \text{Mass of empty container})}{\text{Volume of container}} \quad (4)$$

2.3.10. Biochar yield

The extent of biomass conversion to carbonaceous biochar was indicated by the mass yield that is given by Eq. 5, as reported by Khater et al., 2024.

$$\text{Biochar yield}\ (\%) = \left(\frac{\text{Mass of biochar from pyrolysis}}{\text{Mass of CRD biomass taken for pyrolysis}}\right) \times 100 \quad (5)$$

2.3.11. Higher heating value (HHV)

The HHV of CRD biomass and biochars were calculated using the method described in *Channiwala and Parikh, 2002* and Khatibi et al., 2023. This method correlated elemental analysis to determine fuel-like properties of the materials.

2.3.12. SEM-EDX

All 4 PR:2 biochars were submitted internally to the microscopy laboratory at I^2E,[3] UQTR for the SEM-EDX analysis using a Hitachi electron microscope SU-70 attached to an X-ray analyzer. Magnifications of 500× and 1000× with a 15 kV acceleration voltage under vacuum were adopted for this characterization.

2.4. Statistical analysis

To evaluate the impact of a pyrolysis parameter on key biochar properties such as carbon, hydrogen, oxygen, H/C, O/C, surface area, biochar yield, VC, FC, ash, and TSF, a one-way analysis of variance or ANOVA statistical test using Design Expert software and Origin was applied. Here, differences across the aforesaid dependent variables w.r.t an independent variable like pyrolysis temperature are quantitively analyzed. The data was initially prepared to include replicate information for calculating mean and standard deviation. The *p*-value was then calculated to check the level of significance ($p \leq 0.05$ – the influence is significant) for the ANOVA test. The meaning for errors were also given to understand the cause of outliers.

2.5. Slow pyrolysis of CRD wood residues

2.5.1. Laboratory-scale horizontal tube furnace - 105 min cycle with 60 min BRT

Initially, 15 g of CRD wood waste not cleaned for AAEM and consisting of a heterogeneous mixture of bark-less hardwood and softwood of varying particle sizes (3 mm to 2.5 cm), were loaded into a cylindrical quartz column (length of 12 in., diameter of 1 in., and volume of 0.15 L) of a Thermo Scientific Lindberg Blue M™ 1100 °C mini horizontal tubular fluidized reactor, with a heater wattage of 800 W, power 50/60 Hz and 120 *V*. The unit and its functions are shown in Supplementary figure 2.

It was verified *via* a Mettler Toledo analyzer that the moisture content of biomass was <10 % to minimize a delay in the onset of pyrolysis and to attenuate excessive thermal inertia between the feed and the furnace. Successively, the tube was purged with nitrogen gas (0.1–1 l/min) to flush out oxygen and other reactive gases surrounding biomass, to maintain an inert atmosphere before and after the heating function was turned on. As in Table 1, pyrolysis temperature (300–700 °C) and heating rate (20–50 °C/min) were the variable parameters taken into consideration. In all, 5 experimental runs were conducted to understand the behaviour of the tube furnace on biomass as well as biochar's yield and characteristics. A total cycle time of 105 min was followed during pyrolysis that comprised of a ramp-up phase in the first 15 min, followed by a stationary phase (at set temperature) for 60 min, and a final dwelling/cooling phase for 30 min. The pyrolysis gases generated were condensed in a cold trap and the NCGs were let out.

Table 1
Pyrolysis parameters for laboratory-scale horizontal tube furnace (105 min and 165 min cycles).

Parameters varied during the first round of laboratory trials with constant mass (15 g) of feedstock	Range				
	lowest	low	mid-point	high	highest
Pyrolysis temperature (°C)	300	400	500	600	700
Biomass heating rate (°C/min)	20	26.7	33.3	40	46.7

2.5.2. Laboratory-scale horizontal tube furnace - 165 min cycle with 120 min BRT

For the next series of experiments, the same process conditions as before were adopted except the BRT parameter which was increased to 120 min from 60 min.

2.5.3. AAEM reduction in CRD wood

The sourced CRD biomass while classified as low-ash (<5 %), contains significant intrinsic AAEM that could pose challenges in biochar production by increasing ash content, catalyzing carbon cracking, and reducing fixed carbon, particularly at high pyrolysis temperatures. Initial experiments with untreated CRD wood revealed issues such as residue buildup that required labour-intensive cleaning. Sometimes, it lead to equipment damage and operational downtime in both laboratory and scaled-up reactors. Albeit, a mild acid pre-treatment leached some AAEM content and enabled smoother pyrolysis operations with improved equipment longevity. Given the scarcity of research on CRD wood pyrolysis in Québec and Canada, future work linked to this article will also focus on uncleaned feedstock processed in tube furnaces and pilot-scale equipment (15–25 kg batches) to further investigate the role of pyrolysis parameters, feedstock composition, kinetics, and the operational impact of AAEM-laden wood on biochar properties.

Pre-treatment of CRD biomass to lower AAEM and unstable metal content in ash could increase efficiency of pyrolysis (Mazerolle et al., 2019). To evaluate if AAEM can be reduced in CRD wood residues prior to pyrolysis, solvent-based lixiviation was followed. This washing of biomass involves a systematic approach using specific reagents and methods to ensure effective inorganic contaminant removal. The protocol mentioned in *Québec, 2023* was adopted and modified according to our objectives to be assessed. In Supplementary Fig. 3, CRD wood blocks (base case) and their chipped/milled residues were taken as two different samples just to compare the change in leaching efficiency with particle size and solvent medium. DMW of a neutral pH at 7.00, served as the primary washing solvent. For acid treatment, a solution was prepared by mixing 14 mL nitric acid (HNO_3) and 16 mL of sulfuric acid (H_2SO_4) in a beaker. This stock solution was then diluted by adding it dropwise to 950 mL of DMW in a 2 L beaker, ensuring a final pH range of 3–4 to mimic a moderately acidic leaching (used interchangeably here with lixiviation) atmosphere. Firstly, for DMW as the leaching solvent, 40 g of undried CRD wood as blocks and chips, were loaded into a lixiviation bottle where a solid-to-liquid ratio of 1:4 was maintained. The mixture was stirred vigorously and subjected to a lixiviation roller treatment at 30 rpm for either 16 or 24 h, depending on the

experimental conditions designed. Post-lixiviation treatment, vacuum filtration *via* a 0.45 μm pore size filter paper proceeded to collect the leached filtrate for analysis. Secondly, for acid leaching, the same procedure was followed by substituting DMW with the prepared acid buffer solution as a new lixiviation solvent. For the entirety of experiments, critical parameters including solid-liquid ratio, lixiviation time, rpm, and the weight of CRD chips/blocks, were maintained as constant parameters to ensure reliable results.

2.5.4. Scaled-up horizontal tube furnace

Acid-washed and chipped CRD wood of varying particle sizes (till 2.5 cm) was loaded into a scaled-up horizontal fluidized bed reactor depicted in Supplementary Fig. 4. A BRT of 120 min and pyrolysis temperatures between 300 °C and 800 °C were tested, with heating rates varying from 20 to 55 °C/min to resemble prior conditions. Pyrolysis gas release was monitored as in Supplementary Fig. 5 to check the reaction's progress.

2.5.4.1. Experimental set-up. A Thermo Scientific Lindberg Blue M™ 1100 °C horizontal tube furnace was utilized as a scaled-up configuration for slow pyrolysis under fluidized conditions. A cylindrical heat-resistant steel reactor column of diameter 2.5 in., length 69 in., and a combined volume of approximately 5.55 L, was designed and constructed. It could accept up to 500 g of feedstock for pyrolysis at once considering limitations circumventing heat distribution, inert gas passage, and the circulation time of pyrolytic gases. Heating rate for pyrolysis was calculated based on the fact that the reactor was pre-programmed to achieve the set point temperature (SPT) in 15 min. This instrumentation was equipped with 3 temperature controllers, connected by individual K-type thermocouples that measured the furnace temperature supplied to 3 different zones of the quartz tube reactor. This enabled us to comprehend the actual temperature imbibed by the pyrolysis feedstock keeping in mind, any thermal inertia that may have occured. Supplementarily, another K-type thermocouple was lodged into the quartz column to monitor real time temperature within the reaction zone and to understand how thermal inertia affected the efficiency of pyrolysis. This was the first amendment to our process design. To subdue the settling of hydrocarbon-rich volatiles on biochar surface and also to improve the Van-Krevelen parameters, carefully increased nitrogen flow rates (between 1 and 5 l/min) to sweep through the reactor to flush out any reactive atmospheres and fixing a vacuum pump as in Supplementary Fig. 6 with heating a high suction capacity towards the exit gas zone, were two other measures considered.

A problem *via* accumulation of condensed volatiles in the vacuum suction unit's hose was encountered as pyrolysis gas temperature reduces. A heating tape set at 300 °C and that was attached to the outer body of the vacuum pump's hose, ensured a drastic reduction of tar accumulation inside it or the pump's core. In other words, the pyrolysis gases were transported to the combustion chamber as is with negligible condensation. Usually, if the condensable pyrolysis gases are not removed immediately from the hot reactor, their extended residence time could also result in the formation of more gaseous components thereby leading to carbon loss in biooil or char. The product gases were actually fed into the combustion chamber of a pilot pyrolyzer that catered to a part of its energy demand for pyrolysis operations in the factory. A series of steel meshes with different pore sizes were capped to the end of the reactor column where pyrolysis gases passed through to the vacuum pump. These ensured that firstly, any solid particles were retained within the reactor and did not clog the suction apparatus. Secondly, the meshes also came in handy to prevent solid particulates in the pyrolysis gas mixture from depositing within the condenser train in case they are to be liquified for analyzing the biooil product quality and characteristics.

As the first step to test the column's functions, understand thermal inertia, and acclimatise/train it to pyrolysis cycles, a few redundant test runs were conducted on the CRD wood feedstock as aforesaid earlier, with a diverse range of temperatures (300–800 °C), BRT (30–120 min), and mass of loaded CRD wood (100–500 g). Once the equipment functionalities and process are standardized, further R&R runs will be performed.

3. Results and discussion

3.1. Slow pyrolysis in laboratory-scale horizontal tube furnace - 105 min cycle with 60 min BRT

The three phases of CRD wood pyrolysis, *i.e*, ramp-up, stationary, dwelling, and their experimental progress were recorded as shared in Supplementary Fig. 7. The ultimate analysis and biochar yield data in Table 2 show a clear increase in carbon content with rising pyrolysis temperatures from 300 °C to 600 °C, consistent with observations by Babu et al., 2024. However, at 700 °C, carbon content decreases slightly below 80 %, potentially due to the onset of carbon cracking, resulting in the loss of carbon as light gases. This phenomenon aligns with findings by *Aktas et al. 2024*, which indicate a 39 % reduction in biochar yield—from 39.13 % at 300 °C to 23.93 % at 700 °C. The presence of AAEM in the biomass could have contributed to greater catalytic activity, promoting gas-phase reactions that remove carbon during volatile-char interactions (Li et al., 2023). Conversely, AAEM may also increase secondary char yield under certain conditions, highlighting the complexity of its dual effects (Anca-Couce et al., 2017). Further research is necessary to fully understand these mechanisms.

The density and diversity of oxygen-containing volatile functional groups decrease with rising pyrolysis temperatures. However, at 700 °C, the oxygen content in biochar contradicts this trend, showing an unexpected increase compared to the biochar at 600 °C. This anomaly may result from the deposition of oxygen-rich pyrolytic volatiles on biochar or their interaction during volatile evolution within the reaction zone (Huang et al., 2020). Without proper removal of pyrolytic volatiles—either by increasing the inert carrier gas flow rate or employing vacuum suction—oxygenic volatiles might condense within cooler reactor zones, particularly at the tube's ends where heating is less effective. Additional factors contributing to the observed carbon loss and oxygen increase include: air infiltration during pyrolysis (Supplementary fig. 10); air infiltration during the cooling phase; or secondary reactions between volatiles and char, leading to carbon loss as gaseous products.

Proposed solutions to mitigate these challenges are discussed in subsequent sections, which focus on scaled-up experiments using a horizontal tube furnace.

Table 2
Elemental analysis and biochar yields from the 105 min cycle.

Sample (Biomass or biochar)	N (%)	C (%)	H (%)	S (%)	Ash (%)	O (%)	H/C	O/C	Biochar yield (g)	Biochar yield (%)
CRD wood feed	0.99	49.88	6.12	0.10	1.17	41.74	1.47	0.63	–	–
Biochar at 300 °C	0.30	69.97	3.87	0.17	4.82	20.87	0.66	0.22	5.87	39.13
Biochar at 400 °C	0.38	75.16	3.45	0.09	5.99	14.93	0.55	0.15	4.59	30.60
Biochar at 500 °C	0.39	79.28	2.97	0.05	6.80	10.51	0.45	0.10	4.19	27.93
Biochar at 600 °C	0.34	82.86	2.22	0.03	6.32	8.23	0.32	0.07	3.90	26.00
Biochar at 700 °C	0.57	79.18	1.40	0.02	6.96	11.87	0.21	0.11	3.59	23.93

The removal of heat-labile functional groups (hydrogen, oxygen, and decomposable carbon) increases with higher pyrolysis temperatures and BRT that can be represented by a Van Krevelen diagram. This indicates a reduction in volatile functionalities and progress in carbon structural ordering (C—C, C═C). Low H/C and O/C ratios are critical for oxidative stability, though they require further validation for accurately predicting biochar's structural framework (Zhu et al., 2023). Optimization of pyrolysis conditions and biomass pre-treatment (*e.g.*, acid washing to reduce catalytically active AAEM) can improve biochar quality. Higher temperatures and longer BRT enhance intra-particle heat distribution, aided by external convective heating. This promotes more efficient biomass decomposition, increasing carbon content while reducing oxygen, hydrogen, and overall biochar yield.

To study the effect of longer biomass residence time (BRT), it was increased from 60 to 120 min, keeping the ramp-up and dwelling times constant. The stationary phase (SPT) was extended by 60 min, while the temperature range (300–700 °C) and heating rates remained unchanged. Increasing the nitrogen gas flow is recommended to prevent condensation of pyrolytic volatiles on biochar. However, excessive nitrogen flow may cool the reactor, reducing heat distribution and accelerating volatile condensation.

3.2. Slow pyrolysis in laboratory-scale horizontal tube furnace - 165 min cycle with 120 min BRT

Similar to the 105 min pyrolysis cycle, the three phases of CRD wood pyrolysis in the 165 min cycle with their temperature profiles were recorded as shared in Supplementary Fig. 8. During the 165 min cycle, biochar at 700 °C showed higher carbon content (83–84 %) with reduced oxygenates and improved Van Krevelen parameters of H/C and O/C (Table 3), compared to minor discrepancies in the 105 min cycle. Carbon content increased from 62.16 % at 300 °C to 83.51 % at 700 °C. While increased BRT theoretically reduces yields due to prolonged heating, yields were consistent between cycles at 400–700 °C. However, at 300 °C, yield increased significantly (70.60 %, 10.59 g), likely due to unconverted CRD wood fractions from uneven heating or temperature gradients (Marti-Rossello et al. 2019). The BET surface area at 700 °C was 139.88 m^2/g, indicating micropore formation from volatile decomposition, compared to a lower surface area (2.67 m^2/g) at 300 °C (Barszcz et al., 2024). Pyrolysis gases (CO, CO_2, and C_1–C_3) released intrinsic carbon, forming structurally ordered microporous networks.

A high nitrogen carrier gas flow rate likely reduced reactive species by quickly removing pyrolytic volatiles, preventing their premature settling on biochar or biomass surfaces and reducing secondary charring. Secondary charring can block micropores and active sites, impairing adsorptive properties (Anca-Couce et al., 2017). Retrofitting a vacuum suction pump to extract pyrolytic gases during production is a potential solution for scaled-up systems to mitigate this issue.

High thermal inertia between the refractory bricks and the tube reactor was observed at higher pyrolysis temperatures (≥500 °C), affecting biochar appearance. At lower temperatures (300–400 °C), unconverted biomass fractions persisted suggesting incomplete biomass breakdown and insufficient pyrolysis. To address these issues, additional tests were conducted using equipment with temperature monitoring (*via* a probe) under the same 120 min BRT. Results confirmed a thermal inertia of approximately 300 °C (Supplementary Fig. 9), which adversely impacts biomass carbonization and biochar physiochemical properties. Despite significant thermal inertia, ash content in biochar increased with temperatures from 300 to 700 °C when BRT was extended by 60 min. Pre-treating biomass with H_2SO_4, HNO_3, or water washing could reduce initial metal content, potentially improving biochar quality. Using a gas analyzer during the initial phase of the 120 min BRT cycle (Supplementary fig. 10) revealed oxygen levels of 15–20 vol %, likely from unnoticed air infiltration due to sealing issues. This could lead to mild combustion, contributing to increased ash and reduced carbon in biochar. Gaseous products like CO and CO_2 were detected, likely from typical decarbonylation and decarboxylation reactions but warrant differentiation from oxygen infiltration. Proper reactor sealing and inert gas use are essential to maintain an oxygen-limited environment (<1 vol% oxygen) and prevent combustion-like reactions, ensuring optimal biochar composition and stability.

Examining the results from 105 min and 165 min cycles, minor discrepancies can be observed with respect to heat loss, heat transfer between biomass particles, and partial settling of volatile matter. On the other hand, elemental analysis and yields of biochar implied that the effect of feedstock composition, optimization of pyrolysis parameters, and modifying reactor/working design can boost the reliability of experimentations. Due to the undependability of obtained results from laboratory-scale horizontal tube furnace linked to unevenness of equipment functions, the next phase of trials were conducted in a scaled-up horizontal tube furnace, but this time, using CRD wood treated for inherent metals like AAEM.

3.3. Impact of CRD wood acid washing

Acid washing of CRD wood was performed to assess its ability to leach metals and its impact on subsequent pyrolysis (*Bindar et al.*, 2024a, b). The leaching efficiencies for Ca, K, Ba, Mg, and Na were significantly higher in acidic media than in DMW, regardless of particle size. The formation of soluble metal complexes through proton displacement in the acid might explain this trend (Usino et al., 2023). The pH of lixiviated acidic filtrates increased over time due to rising metal concentrations, neutralizing the acid's effect. As tabulated in Supplementary Table 2, with CRD wood blocks, metal concentrations rose substantially between DMW (16 h lixiviation) and acid (24 h lixiviation): Na from 18.07 to 69.83 mg/L, K from 2.12 to 28.99 mg/L, Ca from 4.50 to 104.11 mg/L, Mg from 5.58 to 52.55 mg/L, and Ba from 0.011 to 0.125 mg/L. For CRD wood chips, similar trends were observed: Na from 86.56 to 240.09 mg/L, K from 20.87 to 239.39 mg/L, Ca from 80.14 to 719.31 mg/L, Mg from 51.01 to 258.03 mg/L, and Ba from 10.096 to 191.242 mg/L. These results confirm the effectiveness of acid washing in reducing metal content, enhancing its potential for improved pyrolysis outcomes.

Ca was the most leached AAEM across both biomass particle sizes (Fig. 2). Mild acid pre-treatment proved effective in reducing AAEM content in CRD wood with stronger acids likely to enhance this reduction further. Acid treatment destabilized and hydrolyzed biomass polymers like hemicellulose and cellulose, weakening covalent bonds with lignin and AAEM which may improve pyrolysis efficiency (Usino et al., 2023). An unusual trend was noted with Fe levels which increased

Table 3
Elemental analysis and biochar yields from the 165 min cycle.

Sample (Biomass or biochar)	N (%)	C (%)	H (%)	S (%)	Ash (%)	O (%)	H/C	O/C	Biochar yield (g)	Biochar yield (%)	S.Area
CRD wood feed	0.99	49.88	6.12	0.10	1.17	41.74	1.47	0.63	–	–	–
Biochar at 300 °C	0.23	62.16	5.37	0.00	4.8	27.39	1.04	0.33	10.59	70.60	2.67
Biochar at 400 °C	0.43	73.14	3.46	0.00	8.8	14.19	0.57	0.15	4.86	32.40	2.76
Biochar at 500 °C	0.36	78.38	2.77	0.00	9.0	9.48	0.42	0.09	3.97	26.47	99.16
Biochar at 600 °C	0.43	79.98	2.27	0.06	10.1	7.19	0.34	0.07	3.75	25.00	104.5
Biochar at 700 °C	0.54	83.51	1.62	0.00	9.6	4.70	0.23	0.04	3.51	23.40	139.88

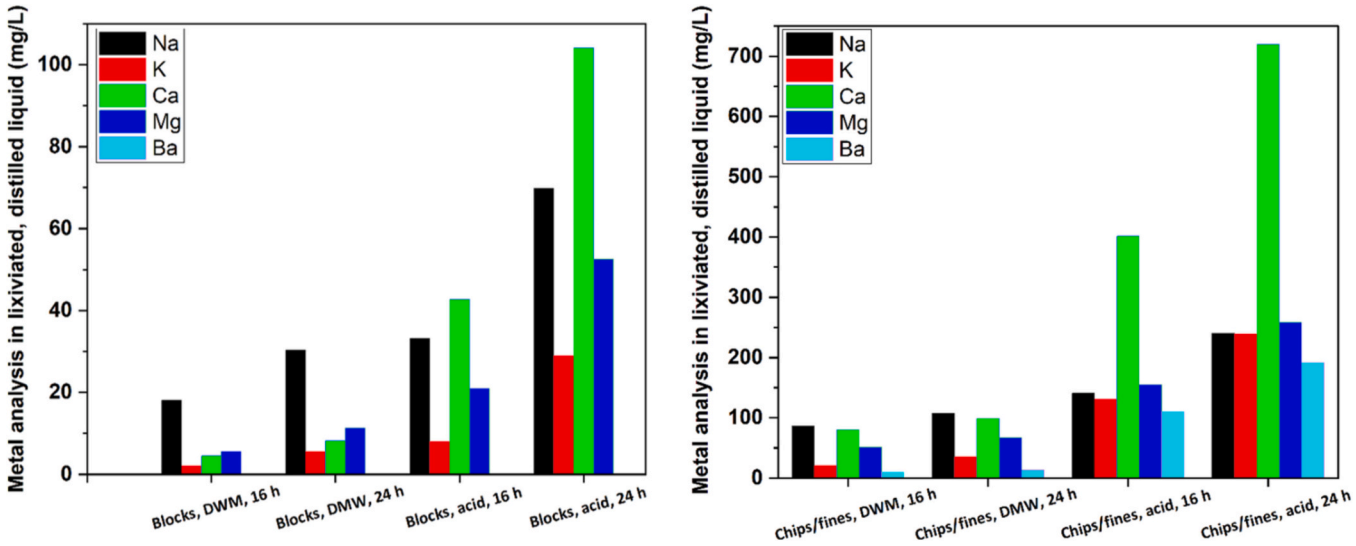

Fig. 2. Variation in concentration of leached AAEM with time, solvent type, and particle size.

Table 4
Difference in composition of CRD wood before and after washing.

Sample (Biomass or biochar)	N (%)	C (%)	H (%)	S (%)	Ash (%)	O (%)	H/C	O/C
CRD wood feed before washing	0.99	49.88	6.12	0.10	1.17	41.74	1.47	0.63
CRD wood feed after washing	0.49	53.83	5.84	0.04	0.85	38.95	1.30	0.54

significantly in CRD wood blocks from 0.82 mg/L (16 h DMW) to 100.77 mg/L (24 h acid). This was likely due to residual nails or metal traces in the blocks, contrasting with lower Fe levels in CRD chips, where particle size reduction helped separate contaminants. Chips also showed higher leaching efficiency, as finer samples provided greater surface area and solution contact.

As described in Zadeh et al., 2020, when the mild acid treated and untreated CRD wood chips were compared, there was an increase in carbon (7.92 %), and a reduction in nitrogen, sulfur, hydrogen, and oxygen heteroatoms as interpreted from Table 4. Implicitly, H/C and O/C were also lowered suggesting that acid treatment solubilized some biomass volatiles. Ash content in the treated fraction concomittantly reduced by 27.35 %.

This experiment, hence proves that AAEM and other metals in CRD wood can be reduced prior to pyrolysis for eliminating any unnecessary side reactions and inflicting mechanical stress over the unit's instrumentation (mainly the reactor). However, it is important to remember that treating CRD wood for any metal removal will generate metal-laden wastewater that has to be treated *via* biological or chemical means eventually adding to process costs.

3.4. Slow pyrolysis in scaled-up horizontal tube furnace

It was examined from Supplementary Fig. 11 that the temperatures of 300 °C and 400 °C yielded low carbon in the biochar and also resulted in incomplete conversion of biomass. In other words, it was increasingly complex to achieve high degree of carbonization below 500 °C. From 500 °C, the conversion and char morphology were appreciable. Higher temperatures of 600, 700, and 800 °C yielded chars with subsided yields, but with superior properties. Subsided yields can be attributed to high heat treatment temperature (HTT) and due to leached/gradual devolatilization of AAEM as inferred from Xu and Sheng, *2012*. Thermal inertia between the refractory bricks and reaction column was minimal (15–20 °C) up to 500 °C but increased to 50–125 °C at 500–800 °C (Supplementary Fig. 12). To address this, SPTs were adjusted for each trial. A 120 min BRT was maintained to replicate conditions from the smaller laboratory-scale setup. At the larger scale, 400 g of feedstock was identified as the optimal biomass load per run, ensuring efficient heat transfer, minimal pyrolytic condensate trapping, and effective inert gas sweeping for vacuum suction. Further experiments are needed to confirm the repeatability and reproducibility (R&R) of this setup.

As a second step, two different conditions were chosen based on the observations from preliminary test runs. For the first condition, a moderate pyrolysis temperature of 500 °C, BRT of 120 min, and 400 g of CRD wood feedstock was adopted. The second condition was executed at a high pyrolysis temperature of 800 °C while the other two parameters remained the same. The elemental analysis and yields of biochar are tabulated in Table 5.

The results in Fig. 3 revealed that CRD wood pyrolysis in the scaled-up horizontal tubular furnace supported lower H/C, O/C, higher carbon, and better temperature control (low heat loss – biomass in the reaction zone received sufficient heat) relative to the laboratory-scale horizontal tubular furnace. So, the next set of trials will be carried forward in this set-up. A comparison of Van-Krevelen performances of CRD wood biochars produced in-house *versus* some reference biochars, anthracites, and cokes (described in Supplementary Table 3) was derived to understand the effect of pyrolysis process conditions on biochar properties.

VC in biochar was estimated as %DB (dry basis) to assess the proportion of easily decomposable carbon. Unlike volatile matter (VM), VC excludes moisture and other labile components. Using ash content values, FC was calculated to better understand carbon stability (Moisture + VC + FC + Ash = 100 wt%). To evaluate the repeatability and reproducibility (R&R) of the scaled-up horizontal tube furnace, two additional pyrolysis rounds (PR:1 and PR:2) were conducted using CRD wood residues from the same bale. Identical biomass pre-treatment and pyrolysis parameters were applied by different operators. The properties of the resulting biochars, detailed in Table 6, were analyzed to validate the system's performance.

3.5. Biochar characterization

3.5.1. Ultimate analysis for PR:1 and PR:2 biochars

Heteroatom composition in PR:1 and PR:2 biochars was consistent. The carbon content increased while oxygen and acidic functionality

Table 5
Biochar properties and conversion from test runs at 500 °C and 800 °C in scaled-up tube furnace.

Sample	N (%)	C (%)	H (%)	S (%)	Ash (%)	O (%)	H/C	O/C	Biochar yield (g)	Biochar yield (%)
CRD wood feed	0.49	53.83	5.84	0.04	0.85	38.95	1.30	0.54	–	–
Biochar 500 °C	0.45	86.26	2.90	0.06	2.66	7.67	0.40	0.07	106.8	26.7
Biochar 800 °C	1.04	90.78	0.72	0.05	6.62	0.79	0.10	0.01	78.0	19.5

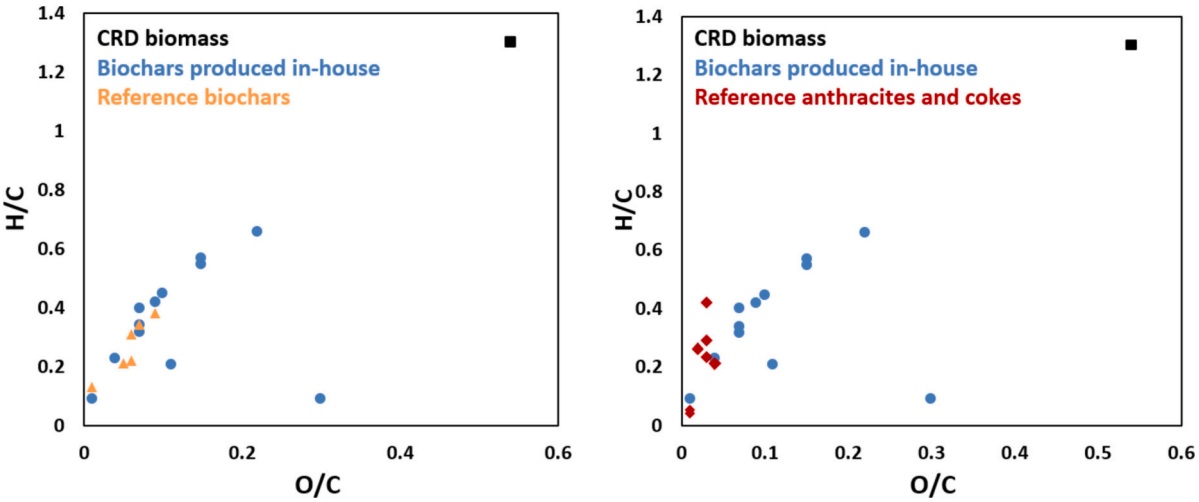

Fig. 3. Comparative Van-Krevelen performance of carbonaceous materials. {**12 tests in total**: (5 tests) - 105 min pyrolysis; (5 tests) - 165 min pyrolysis; and (2 tests) - scaled-up horizontal tube furnace pyrolysis trial runs}.

Table 6
Physiochemical properties of biochars produced in the scaled-up horizontal tubular furnace as part of R&R testing.

Sample	N (%)	C (%)	H (%)	S (%)	Ash (%)	O (%)	H/C	O/C	S.Area (m^2/g)	Pore volume (cm^3/g)	Yield (%)
Treated CRD wood feed	0.49	53.83	5.84	0.04	0.85	38.95	1.30	0.54	–	–	–
Pyrolysis Round 1: (PR:1)											
Biochar 500 °C	0.56	85.42	3.63	0.25	3.88	6.27	0.51	0.06	88.335	0.092	25.7
Biochar 600 °C	0.41	85.46	2.18	1.01	4.94	6.01	0.31	0.05	198.151	0.096	22.4
Biochar 700 °C	0.18	87.82	0.89	0.25	5.88	4.98	0.12	0.04	251.276	0.111	21.1
Biochar 800 °C	0.16	89.54	0.67	0.10	7.27	2.27	0.09	0.02	270.004	0.122	16.6
Pyrolysis Round 2 (PR:2)											
Biochar 500 °C	0.51	84.02	3.11	1.01	2.11	9.24	0.44	0.08	71.354	0.090	26.9
Biochar 600 °C	0.46	85.87	2.64	0.25	3.76	7.02	0.37	0.06	187.516	0.092	21.9
Biochar 700 °C	0.38	87.09	1.59	0.25	5.65	5.04	0.22	0.04	223.703	0.102	19.6
Biochar 800 °C	0.25	89.47	0.91	0.10	6.52	2.76	0.12	0.02	238.88	0.116	15.1

decreased with higher pyrolysis temperatures, promoting aromatic condensation and hydrophobicity. High-temperature biochars exhibited alkaline pH due to the decomposition of surface protons and the concentration of residual ash including AAEM salts and minerals which contribute to basicity (Sun et al., 2017). This alkaline range is beneficial for remediating acidic soils through extractable nitrates, Mg, and Ca (Premalatha et al., 2023). Traces of sulfur from gypsum drywall composites in CRD wood were detected as intrinsic sulfur in biochars at 400–500 °C. After 600 °C, sulfur could have been released as SO_2 and H_2S due to progressive carbon lattice cleavage. Surface area increased significantly with temperature: for PR:1, from 88 m^2/g at 500 °C to 270 m^2/g at 800 °C (206 % rise), and for PR:2, from 71 m^2/g to 238 m^2/g. These enhancements, along with tunable active sites and porosity, make biochar suitable for agricultural applications, improving moisture retention, erosion control, aeration, and microbial development (Sharma, *2024*).

3.5.1.1. H/C and O/C indices to determine biochar stability. Biochars produced at 600–800 °C align with stability standards set by global organizations such as the European Biochar Industry (EBI), International Biochar Initiative (IBI), and Australia New Zealand Biochar Industry Group (ANZBIG) (Adhikari et al., 2024). As shown in the Van Krevelen plots, biochar at 800 °C exhibits properties similar to green coke, with potential for further heat treatment to enhance stability akin to metallurgical or calcined coke. High pyrolysis temperatures increased carbon content while reducing H/C and O/C ratios, consistent with findings by Sanei et al., 2024 and validated in this study. As depicted in Fig. 4, H/C values for biochars above 500 °C dropped to 0.1 or lower, with PR:1 biochar at 800 °C achieving an H/C of 0.09, classifying it under the "inertinite benchmark" (*Bier and Lerchenmüller, 2024*). These biochars hold potential for long-term carbon sequestration, with inertinite fractions offering resistance to degradation for up to 10,000 years (*Bier and Lerchenmuller, 2024*). Although most commercial biochars meet these inertinite criteria, further research is needed to confirm their resistance to microbial degradation through realistic incubation studies (Azzi et al., 2024).

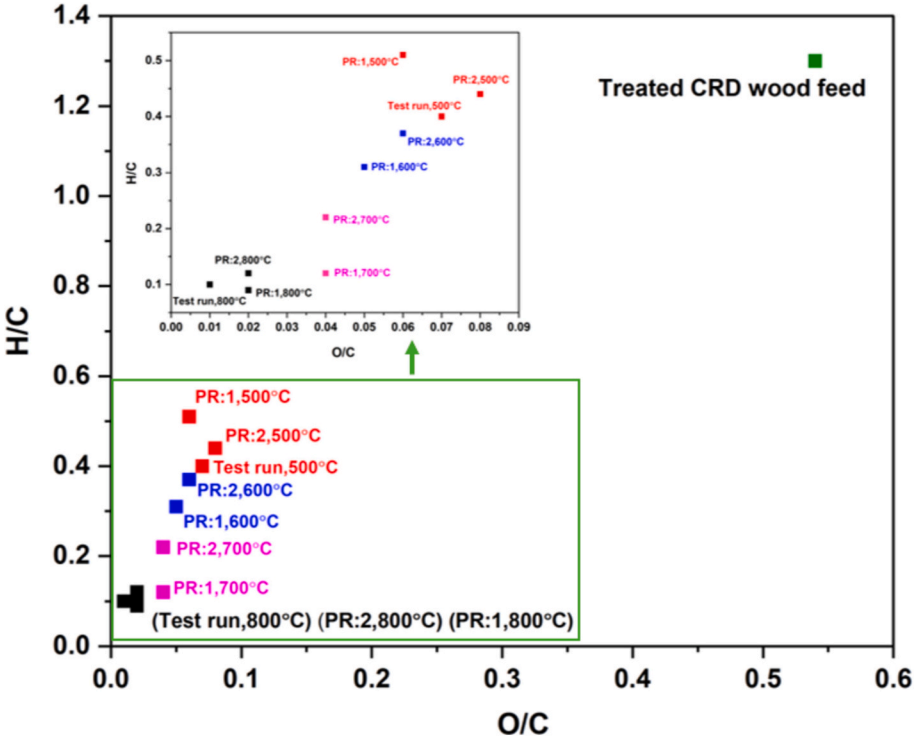

Fig. 4. H/C and O/C indicators of biochars produced in pyrolysis rounds 1 and 2 for projecting stability. The two test runs at 500 °C and 800 °C from laboratory scaled-up horizontal tube furnace are also included.

In the black carbon continuum, biochars with O/C < 0.2 are less sensitive to oxidative atmospheres and may have a half-life exceeding 1000 years, compared to 100–1000 years for O/C between 0.2 and 0.6, and ~ 100 years for O/C > 0.6 (Spokas, *2010*). This makes O/C < 0.2 ideal for applications like soil carbon sequestration and metallurgy, which require resistance to mineralization. Mineralization, as defined in this context, refers to the decay of organic matter to CO_2 *via* biotic or abiotic interactions (*Chiaramonti et al., 2024a, b*). For biochars produced in the scaled-up horizontal tube furnace, O/C values <0.1 (Fig. 4) suggest a minimum half-life of 1000 years and progression towards a turbostratic structure of condensed heterocyclic aromatics. However, confirming this requires molecular analyses such as Raman spectroscopy, XRD, ^{13}C NMR, or FTIR. O/C is an indicator of stability but can be influenced by post-production factors like cooling method, rate, and storage. For instance, while nitrogen-purged cooling and airtight storage in this study ensured O/C < 0.2, air or water cooling and open storage could increase O/C, regardless of pyrolysis temperature. Thus, O/C (and H/C) may reflect not just volatile content but also inherent structure and post-production effects, emphasizing the need for controlled pyrolysis, activation (if necessary), and storage practices.

Table 7
Proximate analysis parameters and HHV for biochars produced in pyrolysis rounds 1 and 2. TGA thermal stability index and Raman index for biochars produced in pyrolysis round 1 only.

Char sample	VC (% DB)	Ash (% DB)	FC (% DB)	TSF (%)	HHV (MJ/kg)	TGA R50	I_D/I_G
PR:1, 500 °C	25.74	3.88	70.38	73.22	33.38	–	–
PR:2, 500 °C	24.86	2.11	73.03	74.60	32.09	0.544	0.787
PR:1, 600 °C	15.55	4.94	79.51	83.64	31.77	–	–
PR:2, 600 °C	16.04	3.76	80.20	83.33	32.30	0.577	0.812
PR:1, 700 °C	12.23	5.88	81.89	87.01	31.09	–	–
PR:2, 700 °C	13.60	5.65	80.75	85.59	31.66	0.588	0.928
PR:1, 800 °C	9.27	7.27	83.46	90.00	31.67	–	–
PR:2, 800 °C	10.06	6.52	83.42	89.24	31.89	0.647	0.972

3.5.2. *Proximate analysis for PR:1 and PR:2 biochars*

In Table 7, increase in pyrolysis temperature from 500 °C to 800 °C, led to a reduction in VC by 64 % among the PR:1 biochars (also described in Supplementary Fig. 13). A similar trend was observed for the PR:2 biochars where it decreased by 60 %. Heat treatment releases most functional groups from the biochar's surface into the pyrolysis gas phase and concentrates carbon with inorganics. This statement can be confirmed by the increase in ash content by 87 % and 209 % for PR:1 and PR:2 biochars respectively. FC concomittantly rose by approximately 19 % and 14 % too.

TSF is a proxy for biochar FC and VC which are in turn surrogate indices for the overall biochar stability. TSF for biochars in PR:1 and PR:2 are comparable and vary from 73 to 75 % when the pyrolysis temperature is 500 °C, to 89–90 % when produced at 800 °C. This could prove that biochars derived at high temperatures can retain a remarkable amount of carbon by resisting thermal decomposition, and could have a high permeance when applied to soils or used for carbon credits projects. HHV of CRD biomass was calculated to be 21.62 MJ/kg. As pyrolysis temperature was increased, the HHV ranged from 31 to 34 MJ/kg which signifies a jump in calorific value. To summarize, the properties of biochar from the above trials (test runs, PR:1, and PR:2) do not differ drastically thereby, bypassing the need for the triplicate runs. There is plausible precision with the results from the two trials in addition to the test runs at 500 and 800 °C. Hence, this equipment is suitable for biochar production.

The following characterizations inclusive of TGA/DTG, SEM-EDX, TGA R50, FTIR, and Raman analysis were performed only on PR:2

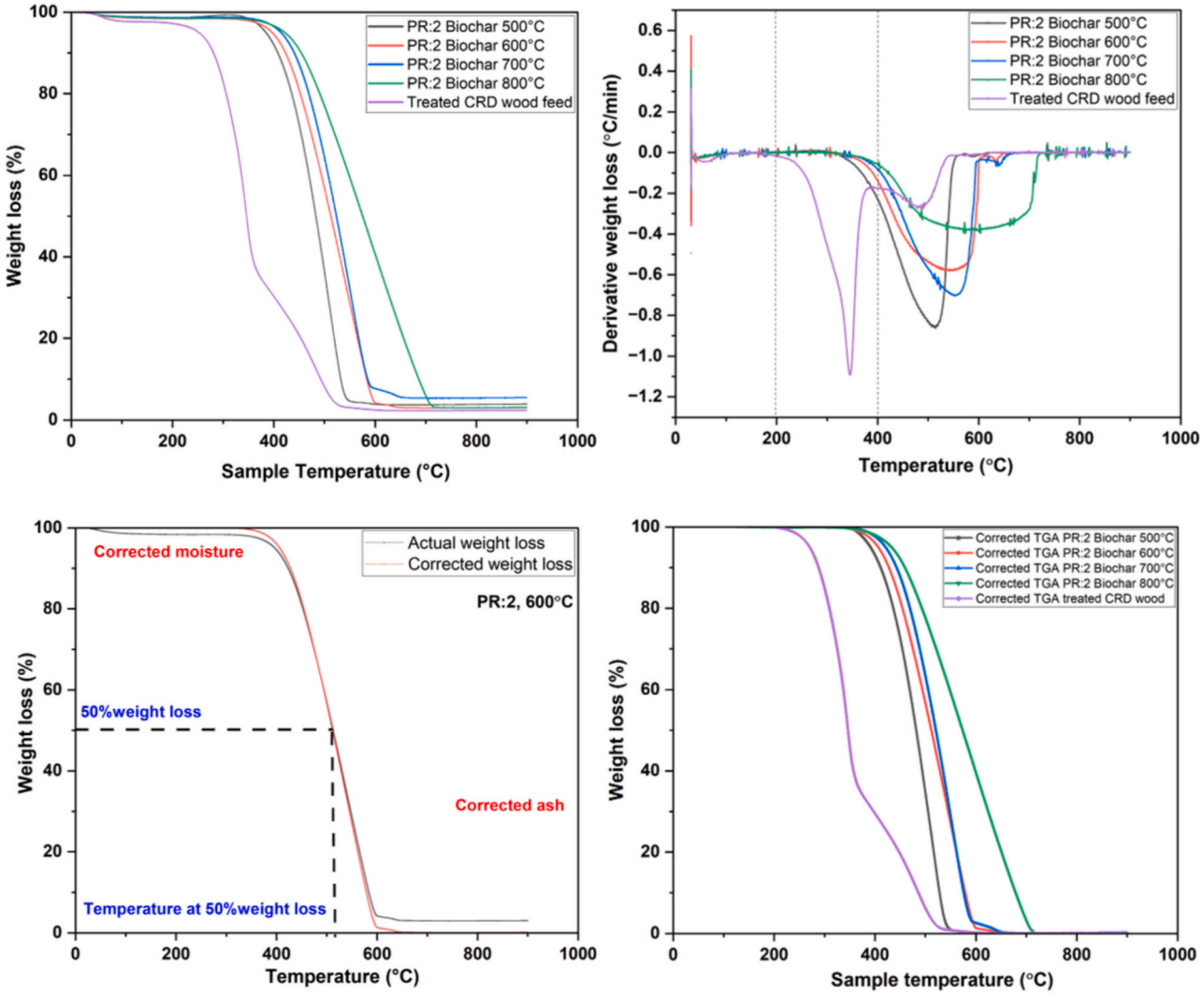

Fig. 5. Top left and right: TGA; and DTG thermal decomposition profiles - for CRD wood biomass and biochars under varying pyrolysis temperatures. Bottom left and right: Sample of a corrected thermogram for calculating the TGA R50 recalcitrance index; and all moisture, ash-corrected thermograms.

biochars as an example to evaluate their stability.

3.5.3. TGA/DTG

Thermal decomposition and stability of biomass and biochars was analyzed using TGA and TGA R50 respectively, at a heating rate of 10 °C/min (Figure 5). Biomass thermograms exhibited a three-phase weight loss pattern (Sarkar et al., 2024): a) water evaporation; b) decomposition of holocellulose (hemicellulose and cellulose); and decay of lignin along with high molecular weight compounds. Maximum biomass weight loss (>90 %) occurred between 150 and 550 °C, while biochars decomposed primarily between 500 and 700 °C, beyond which inorganic content acted as a heat dissipation barrier, halting further weight loss (Anand et al., 2023).

For CRD wood, the DTG plot revealed three degradation phases, similar to pine wood and sawdust (Mishra and Mohanty, *2018*). The first phase (150–200 °C) involved moisture and surface volatile removal. The second phase (200–400 °C) with a sharp weight loss and peaking at 346 °C indicated hemicellulose and cellulose decomposition, accompanied by reactions such as decarbonylation, depolymerization, and decarboxylation, releasing carbon, oxygen, and hydrogen as gas-phase products. This stage marked a significant reduction in char yields and the release of pyrolytic volatiles (condensible as biooil), mostly from cellulose. Progression of pyrolysis is very obvious in this zone where dissociation of the relatively tough lignin framework also begins. The third phase (beyond 400 °C) involved slow lignin decomposition, peaking at 483 °C. Endothermic reactions such as dehydration, cracking, demethylation, condensation, isomerization, and aromatization formed aromatics and higher hydrocarbons. This phase also promoted char formation and residual ash accumulation.

For PR:2 biochars produced at 500–700 °C, the DTG plot showed a single peak mass loss at 515 °C, 539 °C, and 556 °C, reflecting increased thermal stability and higher energy required to break condensed aromatic structures as pyrolysis temperature rose. These biochars exhibited high energy content due to strong C—C, C═C, and C≡C bonds. At these temperatures, diminished H/C and O/C ratios confirm the volatilization of heat labile compounds during carbonization (Babinszki et al., 2024). Slow pyrolysis heating rates promoted VM melting, aiding micropore structure development and surface area increase. Conversely, biochars at lower temperatures retained higher VM, aligning with our findings. For biochar at 800 °C, peak mass loss shifted to ~600 °C, indicating expanded FC and ash content. The flatter DTG curve suggested the absence of easily degradable organics.

3.5.4. SEM-EDX

Through the EDX spectra, the presence of high carbon and resolute AAEM in ash were shown to be predominant contenders in these stable biochars produced at 600–800 °C which is explainable by increase in alkalinity up to a pH of 11.09. Carbon content in the cross-sections of

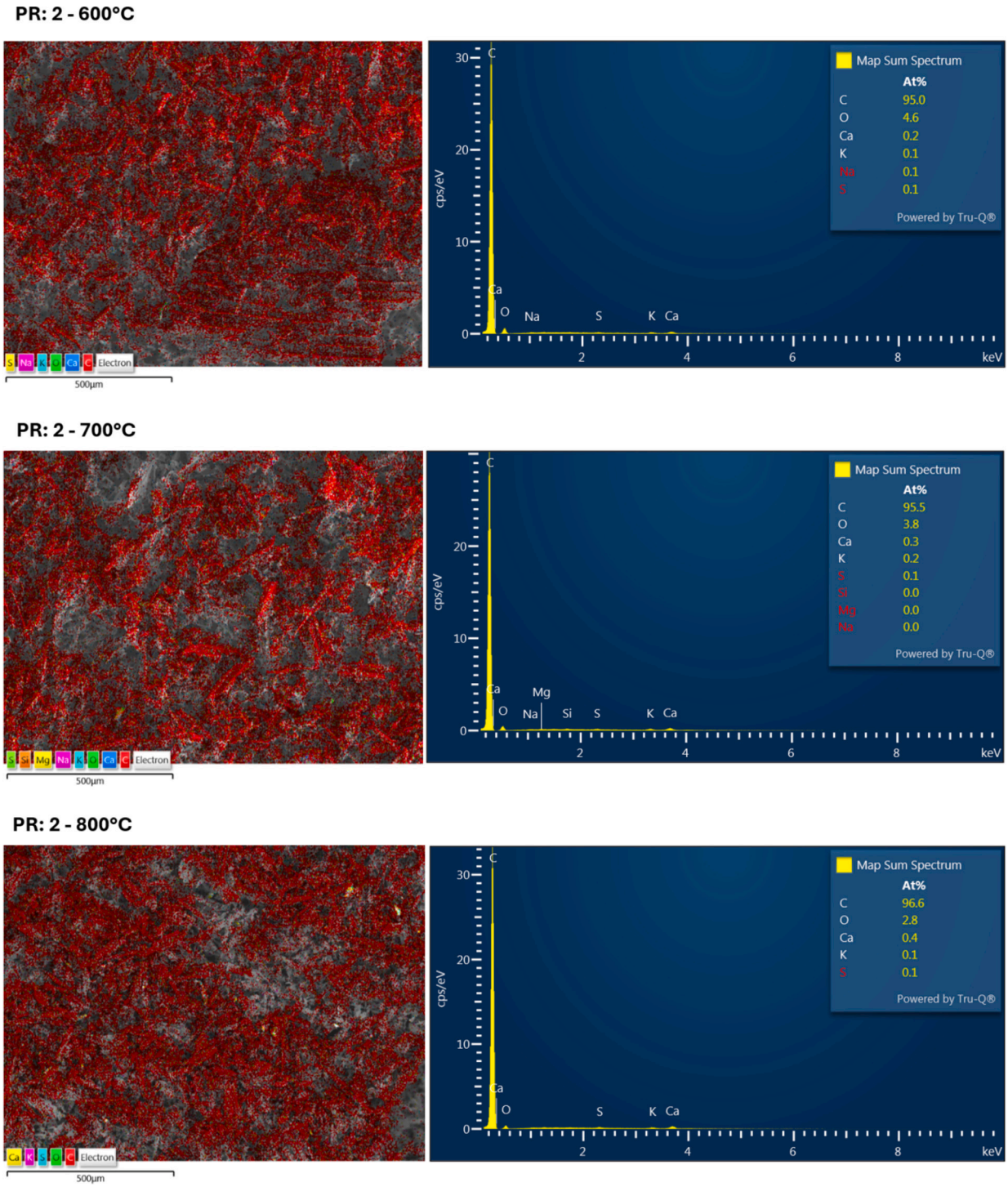

Fig. 6. EDX spectral distribution of biochars with concentrated carbon and reduced volatile content: From the top: 600–800 °C.

biochar under analysis as in Fig. 6, was about 95 %, 95.5 %, and 96.6 % respectively iterating to the formation of large aromatic carbons *via* condensation of small aromatic units. Oxygen decreased from 4.6 % to 3.8 %, and 2.8 % respectively, specifying that high temperatures showed a reduction in oxygenic functional groups (eg: -OH, SO_3H, -COOH). Oxygen may also be bonded to AAEM, as concluded in *Chiaramonti et al., 2024a, b*. AAEM content in ash at this point was mainly seen as Na, K, and Ca making up to 0.4–0.5 % only, due to their eventual devolatilization. Pre-treatment of CRD wood might have also led to a decrease in inorganics detected in the EDX spectra. Sulfur was detected due to the presence of gypsum fines from dry wall residues in the initial CRD wood feedstock.

3.5.5. *TGA R50*

The TGA R50 plots and corrected thermograms (Figure 5) showed improved biochar thermal stability as pyrolysis temperature increased from 500 °C to 800 °C during PR:2. The R50 index rose from 0.54 to 0.65, indicating enhanced stability. Since CRD wood biomass has a R50 of only 0.39, biochar at even a lower temperature can alleviate major stability concerns. As appended in Supplementary Fig. 14, R50 strongly correlates with O/C ratios, where O/C decreases from 0.08 to 0.02 across biochars with increasing HTT, reducing oxidative sensitivity,

promoting the degree of recalcitrance, and minimizing carbon loss to degradative reactions. These findings align with Leng and Huang, 2018, who described a black-carbon continuum where O/C decreases from raw biomass charcoal, combustion soot, and finally to graphite (1 to 0: decreasing order). Biochar, being heterogeneous, overlaps with the other carbonaceous materials in composition and stability. R50 also directly relates to ash, FC, TSF, I_D/I_G, and inversely to VC. However, limitations exist in using R50 as a stability index. Nair et al., 2020 noted that correcting raw thermograms for ash might overlook catalytic inorganics' role in stability. Additionally, R50 for graphite is not constant and varies with experimental conditions, including graphite type, oxygen flow rate, heating rate, and equipment thermal inertia. Measuring graphite R50 alongside biochar samples is essential for consistency. *Gomez et al. 2016* proposed refining the R50 scale as T50 % weight loss for graphite (886 °C) may not necessarily replicate the exact structural changes happening in biochars, especially at lower or moderate temperatures.

3.5.6. FTIR

Generally, an inverse relation is construed between pyrolysis temperature and the presence of functional groups where increase in temperatures exhibit biochar with limited functional groups. From the FTIR spectrum of PR:2 biochar at 500–800 °C, it is clear that low pyrolysis temperatures conserve oxygenic functionalities that provide biochar surfaces with an overall negative charge. More the deprotonation of biochar surface, higher the pH, greater the negativity, and higher the cation exchange capacity (CEC) (Sarfaraz et al., 2020). CEC is evident for soil (eg: minerals) and adsorption (eg: heavy metals and cationic dyes) applications mainly. At high temperatures, these surface groups are eliminated which could decrease the conferred CEC. As concluded from the EDX analysis, AAEM and their salts present as part of the ash fraction in high temperature-biochars, may geometrically shield some oxygen functional groups *via* AAEM-O-C linkages which ameliorate their retention concerns. In this case, an intrinsic CEC may persist till the melting of AAEM at very high temperatures after which CEC is highly negligible.

By fitting the data on assignment of FTIR spectral bands in Johnston, *2017* to Fig. 7, from the range of 900–700 cm-^{1}, biochars produced at 500 °C and 600 °C undergo O—H stretch (812–868 cm^{-1} and 807–868 cm^{-1}, respectively) that may result from a mass loss due to the onset of dehydration reactions. For biochar at 700 °C, the O—H stretch lies slightly farther at 935 cm^{-1} that signifies metal-O-H vibrations and bending associated to minerals in biochar (eg: AAEM-O-H). This may highlight the effect of temperature on mineral degradation that detaches O—H and eventually exposes these labile functionalities. Next, C—O stretch for biochars at 500 °C and 600 °C is seen uniquely in the regions of 1164 cm^{-1} and 1153 cm^{-1}. These intense peaks can correlate with the vibrations amidst pyrolyzed carbohydrate fractions in the form of aldehydes, alcohols, ethers, and furfurals. COO^- activation as in amides from proteins and esters is showcased only for biochars at 500 °C and 600 °C along 1578 cm-^{1} and 1550 cm^{-1} and can be attributed to decarboxylation pathways that reject CO_2. In both phenomena, transformations of oxychemicals are apparent where oxygen rejection reactions are being favored. Also, these peaks within 1650–1550 cm^{-1}, may be due to the vibration of C═C that could relate to skeletal vibrations in lignin aromatics as reported by *Chiaramonti et al., 2024a, b*. Strong C═O striations in ketones and carboxylic acids are common to all four biochars in 1701 cm^{-1}, 1701 cm^{-1}, 1735 cm^{-1}, and 1696 cm^{-1}, respectively. Albeit, the intensity decreases for biochars at 700 °C and 800 °C as they may have already started experiencing decomposition of the aforesaid groups due to increase in HTT.

Between 3000 and 2000 cm^{-1}, C—H stretching vibrations with deformations in terminal CH_2 or CH_3 aliphatic hydrocarbons increase for lower temperature biochars. Rising distortions of H-bearing syndicates can hint at the formation of aromatics from these aliphatics by dehydrogenation, condensation (eg: Diels-Alder), and cyclization which leads to a decrease in H/C as justified from the ultimate analysis results. Between 3100 and 3000 cm^{-1}, C—H stretching vibrations in nascent aromatic systems appear as medium-to-low intensity bands in lower temperature biochars pointing out that a stable arrangement of carbon resulting from high degrees of disorder in amorphous carbon, is in progress as soon as the material witnesses sustained heat treatment. For biochars at 700 °C and 800 °C, these bands are not present that could mean a significant portion of carbon in these biochars do not exhibit defects (McCall et al., 2024). However, this do not mean that such C—H contractions are the only qualifying criteria to identify aromaticity in high temperature-biochars (McCall et al., 2024). Even the presence of any substituents in the aromatic rings structure may also lead to vibrations of the C—H planes. Next, within spectroscopic bands in the range of 3670–3200 cm^{-1}, presence of polar -OH groups that are hydrogen-bonded to biochar mostly *via* moisture sorption, are seen for temperatures of 500 °C and 600 °C making them hydrophilic. Due to large pore sizes, there could also be sufficient diffusion of ambient humidity and its further interaction with biochar carbon. At higher temperatures, the polar -OH groups diminish and this is in agreement with Sahoo et al., 2021. Simultaneously, a diffusion limitation comes into play due to disappearance of *meso* and macropores and the origination of micropores. Despite micropores being limiting factors for the entry of surrounding moisture, their surface availability (increase in surface area) could also lead to sorption and contribute to clear spectral bands in this region.

An interesting observation from the FTIR spectra is the absence of bands below 600 cm^{-1} which may usually arise due to vibrational bending of inorganics like Cl, P, and Si according to Nair et al., 2020. Despite ash content between 5 and 8 % for PR:2 biochars at 700 °C and 800 °C, the absence of spectral bands could be due to devolatilization of some of its endogenous components at high pyrolysis temperatures. Therefore, investigating the exact composition of ash at this stage might be necessary to understand which constituents are amplified and become recalcitrant at high temperatures.

3.5.7. Raman spectroscopy

The I_D/I_G ratio from Fig. 8, captures the structural evolution of biochars during pyrolysis. The D band reflects disorder in amorphous carbon caused by edges, vacancies, or functionalities during its transformation to a turbostratic configuration, while the G band indicates sp^2-bonded crystalline carbon, typical of graphite (Xu et al., 2020). The carbon arrangement in turbostratic crystallites however, does not perfectly resemble stacked carbon as in graphite (Amdani et al., 2020). As pyrolysis temperature increased from 500 °C, PR:2 biochars showed a rise in the D band intensity (higher I_D/I_G), indicating increased faultiness in amorphous carbon (Sarkar et al., 2024). This deformity keeps growing proportionally with pyrolysis temperature or any post-production heat treatment till a point where all defect-borne amorphous carbon is converted to large, stable, condensed aromatics that develop inherent chemical and biological recalcitrance during the transformation process (Pusceddu et al., 2017). At 800 °C, PR:2 biochars reached an I_D/I_G of 0.972, suggesting further pyrolysis at ≥900 °C could yield values >1, signalling structural inconsistencies prior to crystalline carbon formation.

Biochars, however, typically exhibit limited graphitization and may remain mildly non-graphitized even with higher heat treatment (Wood et al., 2024). Unlike TGA R50, the I_D/I_G ratio provides insights into the structural makeup and stability of biochar carbon. Results may vary with sample preparation, biochar particle size, and environmental conditions.

A low H/C can also be analogized with high aromaticity and stable biochar carbon as pyrolysis temperature increases (Xiao et al., 2016) (represented in Supplementary Fig. 15). For example, hydrogen elimination reactions inclusive of dehydration, oxidation, and condensation of cyclic hydrocarbons lower H/C suggesting the formation of monoaromatic and polyaromatic hydrocarbon (MAH/PAH) clusters. This

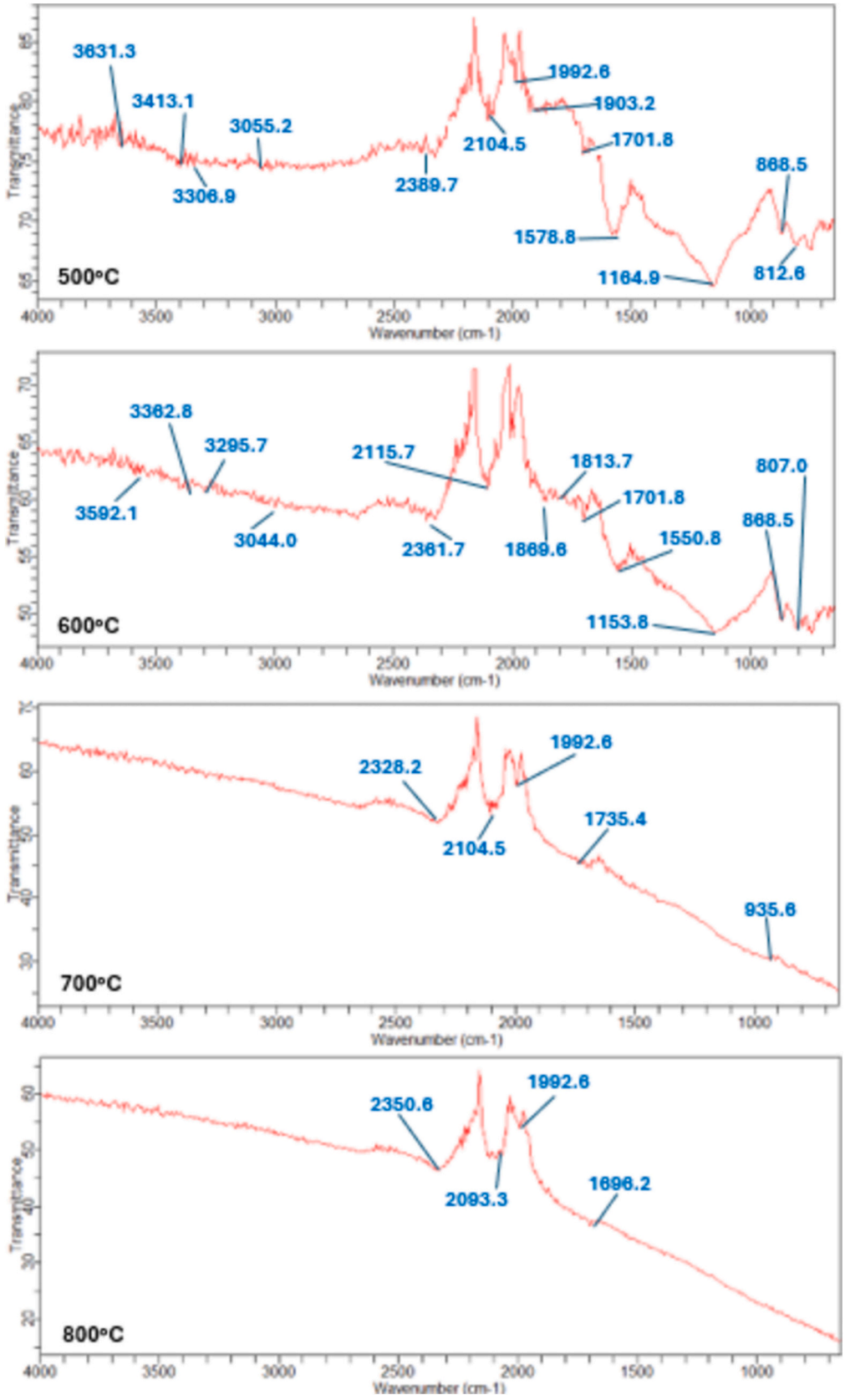

Fig. 7. FTIR spectra and their variations with pyrolysis temperature: Top to bottom - 500-800 °C.

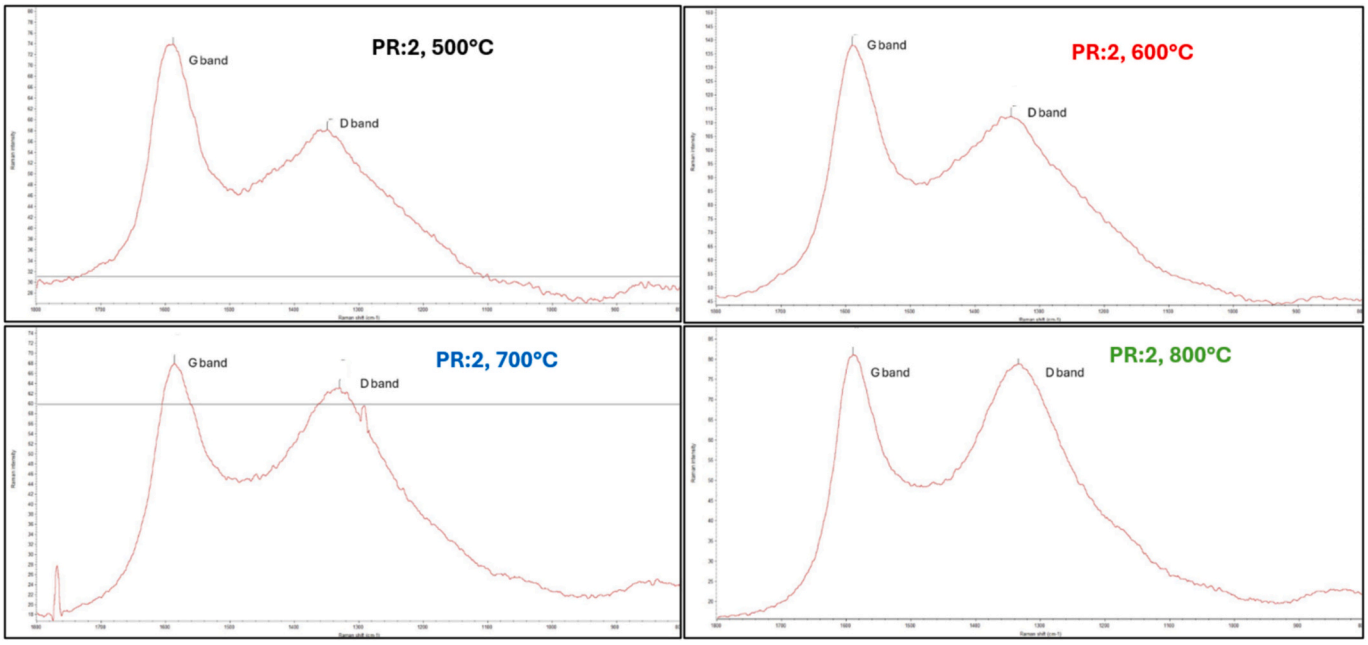

Fig. 8. Defects in biochar carbon with increase in pyrolysis temperature realized *via* the Raman I_D/I_G index. Progress of D band towards G band is from right to left due to inverted x-axis scale. For 500 °C – D band at 1348 cm^{-1} and G band at 1587 cm^{-1}. For 600 °C – D band at 1344 cm^{-1} and G band at 1590 cm^{-1}. For 700 °C – D band at 1330 cm^{-1} and G band at 1586 cm^{-1}. For 800 °C – D band at 1333 cm^{-1} and G band at 1589 cm^{-1}.

theory is ideally validated by the properties of PR:2 biochars where H/C lowered from 0.44 to 0.12, and I_D/I_G graphitization degree increased from 0.787 to 0.972.

3.6. Statistical analysis

The statistical analysis was performed only for biochars from PR:1 and PR:2 produced using the scaled-up horizontal tubular furnace with reference to the most influencing process parameter, *i.e.*, temperature, since other parameters such as BRT, heating rate, equipment, feedstock type, and mass of feedstock processed are unvaried. For a replicate count of two ($N = 2$), a descriptive statistical analysis for biochar properties at each temperature was carried out. The computed values of standard deviations for parameters like C%, H%, O%, H/C, O/C, yield, VC, FC, ash, and TSF of biochar are ≤ 2 (in most cases ≤ 1), which indicates a lower degree of variability among these dependent variables. However, the standard deviation of surface area is >2 that may be due to differences in cross-section of biochar and particle size whilst BET analysis. From the ANOVA analysis, it can be concluded that temperature definitely influenced all dependent variables since *p*-value was ≤ 0.05. With an increase of pyrolysis temperature, a significant elevation of carbon content ($p = 0.004$) especially at 800 °C, decrease in hydrogen ($p = 0.006$) and oxygen content ($p = 0.036$) conferring greater stability and aromaticity, decrease in Van-Krevelen parameters of H/C ($p = 0.005$) and O/C ($p = 0.013$) interspersing resistance towards oxidative reactivity, an increase of surface area ($p = 0.001$) specifically at 800 °C due to micropore development, and a reduction in yield ($p = 0.001$) favoring efficient depolymerization of the CRD biomass, were observed. For the proximate analysis parameters, an increase in temperature aided a drop in VC ($p = 0.0001$), increase in FC ($p = 0.001$), increase in ash ($p = 0.030$), and promotion of TSF ($p = 0.0001$). These replicates also showed very minimal perturbation indicating relatively consistent experimental and characterization conditions.

Any errors in this analysis may have stemmed from minor inconsistencies among CRD biomass constituents taken for pyrolysis mainly at low temperatures, like particle size, composition, and residual inherent contaminants. Sometimes variabilities could arise due to uneven heating patterns encountered in the furnace assembly. Measurement inaccuracies during characterization may be yet another error source. Mitigation strategies to address potential outliers can include increasing the number of replicates and advanced standardization of experimental conditions to enhance data reliability and interpretation. These findings emphasize the importance of optimizing different pyrolysis conditions aside from temperature for desired biochar characteristics.

3.7. Effect of feedstock composition and pyrolysis parameters on biochar properties

To lock in as much stable carbon as possible, the erosion resistance of biochar needs to be remediated such that it does not get oxidised or degraded quickly under harsh environments (natural – *e.g.:* soil, and artificial: power plants). The properties of biochar governing the aforesaid characteristics in general, are greatly influenced by both the type of feedstock, and the conditions appropriated during pyrolysis.

3.7.1. Feedstock composition

3.7.1.1. Biochemical framework. CRD wood residues, a mix of hardwood and softwood, consist of cellulose, hemicellulose, and lignin, with bulk density varying from 200 to 800 kg/m^3, reflecting compositional variability. Their lignin content varied from 24 to 31 % which proves this heterogeneity factor. Softwoods contain 22–40 % hemicellulose, 33–42 % cellulose, and 27–32 % lignin, while hardwoods have 17–38 % hemicellulose, 38–51 % cellulose, and 21–31 % lignin (Tarasov et al., 2018). Hemicellulose, an amorphous polymer of short-chain sugars, decomposes at 190–350 °C, producing non-condensable gases (Wang et al., 2022). Its degradation produces biochar with high volatile content and poor properties (*Chen et al., 2022a, b*). Cellulose, with β-1,4-glycosidic-linked glucose, degrades at 260–400 °C. Amorphous cellulose decomposes first, yielding anhydrosugars like levoglucosan (LGA) and levoglucone (LGO) along with light oxygenates from pyranose ring collapse (Leng et al., 2018). Cellulose contributes to biochar porosity, CEC, and pH, suitable for soil enrichment (Santos et al., 2023). Lignin, a complex aromatic polymer with hydroxyphenyl, syringyl, and guaiacyl units, begins depolymerization at 160–330 °C and undergoes significant

mass loss at 400–600 °C due to stable C═C, C—O, and aromatic bonds (Li et al., 2020). Lignin's aromatic content enhances char yield and stability, with optimal pyrolysis temperatures between 300 and 600 °C. Softwoods, with higher lignin content, favor recalcitrant char formation.

3.7.1.2. Extractives. Additionally, biomass is also embodied of extractive materials such as pigments, sugars, fats, proteins, resins, gums, oils, and waxes that can either effect the reactivity of feedstock during pyrolysis reactions or can block biochar pores thereby reducing its surface area and reactivity (Shadangi et al., 2023). This is implicit for CRD residues that is bearing painted, varnished or resin-rich wood.

3.7.1.3. Inorganics and minerals. Biomass for pyrolysis contains inorganic minerals, including AAEM (*e.g.*, Ca, K, Na, Mg, Ba) and their salts (chlorides, carbonates, sulfates, nitrates), which influence biochar's ash content, porosity, and reactivity (Mourant et al., 2011). AAEMs, acting as cross-linkers in biomass polymers, sever, and reform organometallic bonds (*e.g.*, Ca-O-C) during pyrolysis, altering reaction pathways (Mourant et al., 2011). While AAEMs can enhance secondary char production (Anca-Couce et al., 2017), they also concentrate ash at high temperatures, reducing carbon content (Hu et al., 2015). Additionally, AAEMs promote reactions such as the water-gas-shift (WGS) and Boudouard reactions, increasing CO_2, H_2, and CO in the gas fraction (Hu et al., 2015). Pyrolysis temperature significantly affects biochar pH and surface functionality. At low temperatures, volatiles with protonic functional groups are retained, resulting in acidic biochar (pH $<$ 7). Higher temperatures eliminate H-containing volatiles and concentrate inorganic salts (*e.g.*, $CaCO_3$, KOH, NaCl), leading to negatively charged surfaces and alkaline biochar (pH $>$ 7). This trend was observed in PR:1 and PR:2 biochars, where pH increased from 7.27 to 11.09 as pyrolysis temperature rose from 500 °C to 800 °C.

3.7.2. Pyrolysis parameters: Interdependence between biomass particle size, temperature, heating rate, and BRT to assess potential applications

The CRD wood sized between a few mm and 2.5 cm, showed minimal heat transfer limitations at high pyrolysis temperatures. However, biochars produced at 300 °C and 400 °C in both laboratory-scale and scaled-up horizontal tube furnaces could have faced intra-particle thermal gradient issues particularly at 300 °C, leading to poor conversion. To address this, subsequent trials were conducted starting at 500 °C, ensuring complete carbonization. BET characterization revealed that smaller CRD wood particle sizes increased biochar surface area due to reduced macro- or mesoporosity and enhanced micropore formation (Maziarka et al., 2024). Biochars produced at 700 °C and 800 °C achieved surface areas between 200 and 300 m^2/g without additional activation.

At high pyrolysis temperatures, aromatic compounds fuse, increasing stability as labile functionalities are rejected, and carbon becomes concentrated. Fused aromatic rings stack into carbon sheets, transitioning from amorphous to composite, turbostratic, and ultimately annealed structures with maximum order (Zou et al., 2024; Makowska and Dziosa, *2024*). This progression is reflected in the I_D/I_G ratio from Raman spectra (PR:2 biochar), exceeding 0.9 at 800 °C, indicating deformations in the carbon lattice en route to a graphitic structure. High-temperature biochars (700–800 °C) exhibit enhanced mechanical integrity, carbon content, microporosity, and surface area, making them suitable for metallurgy, pollutant adsorption, capacitive energy storage, soil salinization mitigation, and long-term carbon sequestration (Xu et al., 2024). However, at these temperatures, CRD wood particle yields are lower due to rapid thermal degradation and charring. Achieving a balance between solids yield and carbon composition is critical for effective conversion. For soil amendment applications aiming to reduce nutrient run-off and improve water retention, biochars with greater porosity and surface functionality are preferred. These properties are best achieved at lower pyrolysis temperatures, promoting hydrophilicity and uniform surface features (Tang et al., 2023).

A low heating rate (~50 °C/min or lower) enables gradual phase transformations, balancing biochar yield and gas evolution (Mukherjee et al., 2022). Combined with high BRT, it enhances carbon conservation, FC, low VM, and calorific value, making biochar ideal for metallurgical reductants and power plants (Makavana et al., 2020). From Table 7, biochar produced at 500 °C had the highest HHV, while higher temperatures reduced HHV by 1–2 MJ/kg due to increased ash and reduced hydrogen content (Rahmat et al., 2023). The resulting hydrophobic and stable biochar is suitable for polymer composites, enhancing thermal stability, tensile strength, and impact resistance (Hoang et al., 2024). Hydrophobic biochar has also been applied for oil spill sorption (Sun et al., 2022). Heating rate also influences porosity. Low heating rates, prolonged BRT, and high temperatures for small CRD wood particles result in micropores with high adsorptive properties. For PR:2 biochar at 600 °C, 40 °C/min, and 120 min BRT, adsorption capacity for methyl orange (MO) ranged from 0.8 mg/g to 15 mg/g, achieving >90 % dye removal for wastewater concentrations of 8–164 ppm (Tomczyk et al., 2020). Conversely, higher heating rates with low BRT cause rapid devolatilization, creating macropores suited for agricultural applications but with reduced surface area (Hosseinzaei et al., 2022).

4. Conclusion

The nature of biomass feedstock and pyrolysis conditions penultimately decide biochar's physiochemical properties and potential applications. Slow pyrolysis characterized by low heating rate, high residence time, and high pyrolysis temperature produced highly stable biochar that can be evaluated by different categories of stability indicators. Proximate analysis can be used to derive a conclusion on the chemical make-up of biochar whereas ultimate analysis with the support of Van-Krevelen indices, can predict both the chemical composition and stability of biochar at appreciable levels and moreover, cost-effectively within a short time frame. Structural analysis tools like Raman I_D/I_G, despite being a rapid technique, is expensive. FTIR is very beneficial to identify functional groups of interest on biochar surfaces that gives an overall idea of biochar carbon forms. TGA coupled with DTG and R50 recalcitrance index, are sound methods to evaluate biochar thermal stability but encompass nuances related to the apt heating rates employed during non-isothermal analysis. SEM-EDX can be used as an auxiliary method to proximate and ultimate analysis for assessing ash and carbon concentration in biochar which communicate a proverbial inertness factor, *i.e.,* resistance to biotic and abiotic degradation. Standardizing these metrics and understanding that no single indicator can be exploited to assess biochar permeance are key as part of further investigations especially in the area of CDR technologies. As for future work on CRD wood waste valorization, scaled-up pilot pyrolysis trials to produce biochar followed by its characterization, kinetic analysis of pyrolytic decomposition *via* non-isothermal TGA/DTG under different heating rates, and the propensity for biochar to undergo self-ignition during post-production stages, will be studied.

CRediT authorship contribution statement

Aravind Ganesan: Writing – review & editing, Writing – original draft, Visualization, Validation, Supervision, Software, Methodology, Investigation, Formal analysis, Data curation, Conceptualization. **Olivier Rezazgui:** Writing – review & editing, Supervision, Resources, Project administration, Funding acquisition. **Simon Langlois:** Writing – review & editing, Supervision. **Cyrine Boussabbeh:** Writing – review & editing, Supervision, Resources, Project administration, Investigation. **Simon Barnabé:** Supervision, Resources, Project administration.

Funding

This research was funded by MITACS, through Escouade Energie,

Citeq, and supported by Innofibre, and I^2E^3 – UQTR, Québec, Canada. The work was conducted at Innofibre – Centre d'Innovation des Produits Cellulosiques, Trois-Rivières and at the Institute for Innovation in Eco-materials, Ecoproducts, and Ecoenergies (I^2E^3), University of Québec Trois-Rivières (UQTR), Québec, Canada.

Declaration of competing interest

The authors declare that they have no known competing financial interests or personal relationships that could have appeared to influence the work reported in this paper.

Appendix A. Supplementary data

Supplementary data to this article can be found online at https://doi.org/10.1016/j.scitotenv.2025.178650.

Data availability

The data that has been used is confidential.

References

Adhikari, S., Moon, E., Paz-Ferreiro, J., Timms, W., 2024. Comparative analysis of biochar carbon stability methods and implications for carbon credits. Sci. Total Environ. 914, 169607.

Aktas, Turkan, Dalmis, I. Savas, Taseri, Levent, Batur, Tolga, 2024. a comprehensive character- ization of biochar derived from grape pomace via fast pyrolysis. Int J Sci Res Sci Eng Technol 11 (4), 218–227. https://doi.org/10.32628/IJSRSET24114125.

Amdani, R.Z., Ossler, F., Brackmann, C., 2020, June. Raman spectroscopy for characterizing porous carbon. In: Laser Applications to Chemical, Security and Environmental Analysis. Optica Publishing Group pp.(LTh4F-3).

Anand, A., Gautam, S., Ram, L.C., 2023. Feedstock and pyrolysis conditions affect suitability of biochar for various sustainable energy and environmental applications. J. Anal. Appl. Pyrolysis 170, 105881.

Anca-Couce, A., Dieguez-Alonso, A., Zobel, N., Berger, A., Kienzl, N., Behrendt, F., 2017. Influence of heterogeneous secondary reactions during slow pyrolysis on char oxidation reactivity of woody biomass. Energy Fuel 31 (3), 2335–2344.

Azzi, E.S., Li, H., Cederlund, H., Karltun, E., Sundberg, C., 2024. Modelling biochar long-term carbon storage in soil with harmonized analysis of decomposition data. Geoderma 441, 116761.

Babinszki, B., Czirok, I.S., Johnson, R., Sebestyén, Z., Jakab, E., Wang, L., Czégény, Z., 2024. Volatile matter characterization of birch biochar produced under pressurized conditions. J. Therm. Anal. Calorim. 1–12.

Babu, K.K.B.S., Nataraj, M., Tayappa, M., Vyas, Y., Mishra, R.K., Acharya, B., 2024. Production of biochar from waste biomass using slow pyrolysis: studies of the effect of pyrolysis temperature and holding time on biochar yield and properties. Materials Science for Energy Technologies 7, 318–334.

Barszcz, W., Łożyńska, M., Molenda, J., 2024. Impact of pyrolysis process conditions on the structure of biochar obtained from apple waste. Sci. Rep. 14 (1), 10501.

Bier, H., Lerchenmüller, H., 2024. European Biochar Industry (EBI). Perspectives from two recent publications and EBI conclusions, Report on permeance of biochar.

Bindar, Y., Steven, S., Kresno, S.W., Hernowo, P., Restiawaty, E., Purwadi, R., Prakoso, T., 2024a. Large-scale pyrolysis of oil palm frond using two-box chamber pyrolyzer for cleaner biochar production. Biomass Convers. Biorefinery 14 (5), 6421–6434.

Bindar, Y., Ramli, Y., Steven, S., Restiawaty, E., 2024b. Optimization of purity and yield of amorphous bio-silica nanoparticles synthesized from bamboo leaves. Can. J. Chem. Eng. 102 (4), 1419–1430.

Budai, A., Zimmerman, A.R., Cowie, A.L., Webber, J.B.W., Singh, B.P., Glaser, B., Joseph, S., 2013. Biochar carbon stability test method: an assessment of methods to determine biochar carbon stability. International biochar initiative 1, 1–20.

Channiwala, S.A., Parikh, P.P., 2002. A unified correlation for estimating HHV of solid, liquid and gaseous fuels. Fuel 81 (8), 1051–1063.

Chen, D., Cen, K., Zhuang, X., Gan, Z., Zhou, J., Zhang, Y., Zhang, H., 2022b. Insight into biomass pyrolysis mechanism based on cellulose, hemicellulose, and lignin: evolution of volatiles and kinetics, elucidation of reaction pathways, and characterization of gas, biochar and bio-oil. Combust. Flame 242, 112142.

Chen, J., Wang, P., Ding, L., Yu, T., Leng, S., Chen, J., Zhou, W., 2021. The comparison study of multiple biochar stability assessment methods. J. Anal. Appl. Pyrolysis 156, 105070.

Chen, J., Ding, L., Wang, P., Zhang, W., Li, J., Mohamed, B.A., Zhou, W., 2022a. The estimation of the higher heating value of biochar by data-driven modelling. J. Renew. Mater 10, 1555–1574.

Chiaramonti, D., Lehmann, J., Berruti, F., Giudicianni, P., Sanei, H., Masek, O., 2024a. Biochar is a long-lived form of carbon removal, making evidence-based CDR projects possible. Biochar 6 (1), 81.

Chiaramonti, D., Lotti, G., Vaccari, F.P., Sanei, H., 2024b. Assessment of long-lived carbon permanence in agricultural soil: unearthing 15 years-old biochar from long-term field experiment in vineyard. Biomass Bioenergy 191, 107484.

Cross, A., Sohi, S.P., 2013. A method for screening the relative long-term stability of biochar. GCB Bioenergy 5 (2), 215–220.

Dada, T.K., Sheehan, M., Murugavelh, S., Antunes, E., 2021. A review on catalytic pyrolysis for high-quality bio-oil production from biomass. Biomass Convers. Biorefinery 1–20.

Dieguez-Alonso, A., Anca-Couce, A., Zobel, N., Behrendt, F., 2015. Understanding the primary and secondary slow pyrolysis mechanisms of holocellulose, lignin and wood with laser-induced fluorescence. Fuel 153, 102–109.

Fawaz, M., Avery, A., Onasch, T.B., Williams, L.R., Bond, T.C., 2021. Pyrolysis principles explain time-resolved organic aerosol release from biomass burning. Atmos. Chem. Phys. 21 (20), 15605–15618.

Gómez, N., Rosas, J.G., Singh, S., Ross, A.B., Sánchez, M.E., Cara, J., 2016. Development of a gained stability index for describing biochar stability: relation of high recalcitrance index (R50) with accelerated ageing tests. J. Anal. Appl. Pyrolysis 120, 37–44.

Harvey, O.R., Kuo, L.J., Zimmerman, A.R., Louchouarn, P., Amonette, J.E., Herbert, B.E., 2012. An index-based approach to assessing recalcitrance and soil carbon sequestration potential of engineered black carbons (biochars). Environ. Sci. Technol. 46 (3), 1415–1421.

Hasan, M.M., Rasul, M.G., Khan, M.M.K., 2022, November. The effects of slow and fast pyrolysis on the yields and properties of produced bio-oils from macadamia nutshell. In: AIP Conference Proceedings, vol. 2681, No. 1. AIP Publishing.

Heo, H.S., Park, H.J., Park, Y.K., Ryu, C., Suh, D.J., Suh, Y.W., Kim, S.S., 2010. Bio-oil production from fast pyrolysis of waste furniture sawdust in a fluidized bed. Bioresour. Technol. 101 (1), S91–S96.

Hoang, P., Zhang, Z., Ren, J., Peng, Y., Cao, J., 2024. Versatile biochar for wood-plastic composites: improving mechanical properties, dimensional and thermal stability. Polym. Compos. 45 (11), 10349–10364.

Hosseinzaei, B., Hadianfard, M.J., Ruiz-Rosas, R., Rosas, J.M., Rodríguez-Mirasol, J., Cordero, T., 2022. Effect of heating rate and H3PO4 as catalyst on the pyrolysis of agricultural residues. J. Anal. Appl. Pyrolysis 168, 105724.

Hu, S., Jiang, L., Wang, Y., Su, S., Sun, L., Xu, B., Xiang, J., 2015. Effects of inherent alkali and alkaline earth metallic species on biomass pyrolysis at different temperatures. Bioresour. Technol. 192, 23–30.

Huang, Y., Liu, S., Akhtar, M.A., Li, B., Zhou, J., Zhang, S., Zhang, H., 2020. Volatile–char interactions during biomass pyrolysis: understanding the potential origin of char activity. Bioresour. Technol. 316, 123938.

Johnston, C. T. (2017). 18 biochar analysis by Fourier-transform infra-red spectroscopy. *Biochar: a guide to analytical methods*, 199.

Jung, S.H., Kim, S.J., Kim, J.S., 2012. Characteristics of products from fast pyrolysis of fractions of waste square timber and ordinary plywood using a fluidized bed reactor. Bioresour. Technol. 114, 670–676.

Kasmiarno, L.D., Panannangan, J.K., Steven, S., Rizkiana, J., Hernowo, P., Achmad, F., Bindar, Y., 2024. Exploration of bio-hydrocarbon gases production via pyrolysis of fresh natural rubber: experimental and volatile state kinetic modeling studies. J. Anal. Appl. Pyrolysis 177, 106275.

Khater, E.S., Bahnasawy, A., Hamouda, R., Sabahy, A., Abbas, W., Morsy, O.M., 2024. Biochar production under different pyrolysis temperatures with different types of agricultural wastes. Sci. Rep. 14 (1), 2625.

Khatibi, M., Nahil, M.A., Williams, P.T., 2023. Improving the quality of bio-oil using the interaction of plastics and biomass through Copyrolysis coupled with nonthermal plasma processing. Energy Fuel 38 (2), 1240–1257.

Kim, J.W., Lee, H.W., Lee, I.G., Jeon, J.K., Ryu, C., Park, S.H., et al., 2014. Influence of reaction conditions on bio-oil production from pyrolysis of construction waste wood, renew. Energy 65, 41–48. https://doi.org/10.1016/j.renene.2013.07.009.

Klasson, K.T., 2017. Biochar characterization and a method for estimating biochar quality from proximate analysis results. Biomass Bioenergy 96, 50–58.

Leng, E., Zhang, Y., Peng, Y., Gong, X., Mao, M., Li, X., Yu, Y., 2018. In situ structural changes of crystalline and amorphous cellulose during slow pyrolysis at low temperatures. Fuel 216, 313–321.

Leng, L., Huang, H., 2018. An overview of the effect of pyrolysis process parameters on biochar stability. Bioresour. Technol. 270, 627–642.

Li, B., Huang, H., Xie, X., Wei, J., Zhang, S., Hu, X., Liu, D., 2023. Volatile-char interactions during biomass pyrolysis: effects of AAEMs removal and KOH addition in char. Renew. Energy 219, 119459.

Li, J., Bai, X., Fang, Y., Chen, Y., Wang, X., Chen, H., Yang, H., 2020. Comprehensive mechanism of initial stage for lignin pyrolysis. Combust. Flame 215, 1–9.

Li, S., Chen, G., 2018. Thermogravimetric, thermochemical, and infrared spectral characterization of feedstocks and biochar derived at different pyrolysis temperatures. Waste Manag. 78, 198–207.

Makavana, J.M., Sarsavadia, P.N., Chauhan, P.M., 2020. Effect of pyrolysis temperature and residence time on biochar obtained from pyrolysis of shredded cotton stalk. International Research Journal of Pure and Applied Chemistry 21 (13), 10–28.

Makowska, M., Dziosa, K., 2024. Influence of different pyrolysis temperatures on chemical composition and graphite-like structure of biochar produced from biomass of green microalgae Chlorella sp. Environ. Technol. Innov. 35, 103667.

Martí-Rosselló, T., Li, J., Lue, L., Kärlstrom, O., & Brink, A. (2019, June). Heat transfer behaviour of a wheat straw pellet undergoing pyrolysis. In *ICAE2019: the 11th international conference on applied energy*.

Mazerolle, D., Rezaei, H., Bronson, B., Nguyen, L., Preto, F., 2019. Sieving and acid washing as a pretreatment to fast pyrolysis of a high ash hog fuel. Energy Fuel 33 (6), 5352–5359.

Maziarka, P., Kienzl, N., Dieguez-Alonso, A., Fierro, V., Celzard, A., Arauzo, P.J., Ronsse, F., 2024. Part 1— impact of pyrolysis temperature and wood particle length on vapor cracking and char porous texture in relation to the tailoring of char properties. Energy Fuel 38 (11), 9751–9771.
McCall, M.A., Watson, J.S., Sephton, M.A., 2024. Predicting stability of barley straw-derived biochars using Fourier transform infrared spectroscopy. ACS Sustainable Resource Management 1 (9), 1975–1983.
McLaughlin, H., 2018. Biochar Standards and Characterization Schemes.
Mishra, R.K., Mohanty, K., 2018. Pyrolysis kinetics and thermal behavior of waste sawdust biomass using thermogravimetric analysis. Bioresour. Technol. 251, 63–74.
Mourant, D., Wang, Z., He, M., Wang, X.S., Garcia-Perez, M., Ling, K., Li, C.Z., 2011. Mallee wood fast pyrolysis: effects of alkali and alkaline earth metallic species on the yield and composition of bio-oil. Fuel 90 (9), 2915–2922.
Muema, F.M., Richardson, Y., Keita, A., Sawadogo, M., 2024. An interdisciplinary overview on biochar production engineering and its agronomic applications. Biomass Bioenergy 190 (2024), 107416.
Mukherjee, A., Patra, B.R., Podder, J., Dalai, A.K., 2022. Synthesis of biochar from lignocellulosic biomass for diverse industrial applications and energy harvesting: effects of pyrolysis conditions on the physicochemical properties of biochar. Frontiers in Materials 9, 870184.
Nair, R.R., Mondal, M.M., Weichgrebe, D., 2020. Biochar from co-pyrolysis of urban organic wastes—investigation of carbon sink potential using ATR-FTIR and TGA. Biomass Convers. Biorefinery 1–15.
Oktavia, F.D., Steven, S., Putri, A.H.I., Hernowo, P., Restiawaty, E., Bindar, Y., 2024. Vacuum distillation of raw bio-crude oil (RBCO) from empty fruit bunches (EFB) pyrolysis to produce light distillate containing acetic acid and phenol for sustainable chemical purposes. Braz. J. Chem. Eng. 1–18.
Pahnila, M., Koskela, A., Sulasalmi, P., Fabritius, T., 2024. Biocarbon production using three-stage pyrolysis and its preliminary suitability to the iron and steel industry. Energies 17 (13), 3131.
Panwar, N.L., 2024. Pyrolysis technologies for biochar production in waste management: a review. Clean Energy 8 (4), 61–78.
Premalatha, R.P., Poorna Bindu, J., Nivetha, E., Malarvizhi, P., Manorama, K., Parameswari, E., Davamani, V., 2023. A review on biochar's effect on soil properties and crop growth. Frontiers in Energy Research 11, 1092637.
Pusceddu, E., Montanaro, A., Fioravanti, G., Santilli, S.F., Foscolo, P.U., Criscuoli, I., Miglietta, F., 2017. Comparison between ancient and fresh biochar samples, a study on the recalcitrance of carbonaceous structures during soil incubation. Int. J. New Technol. Res 3, 39–46.
Rahmat, A., Nissa, R.C., Nuraini, L., Nurtanto, M., Ramadhani, W.S., 2023, June. Analysis of rice husk biochar characteristics under different pyrolysis temperature. In: IOP Conference Series: Earth and Environmental Science, vol. 1201, No. 1. IOP Publishing, p. 012095.
Recyc-Québec, 2018. Construction, Renovation, and Demolition Residues (CRD). https://www.recyc-quebec.gouv.qc.ca/sites/default/files/documents/Fiche-info-crd.pdf. Accessed on 1 November 2024.
Recyc-Québec, 2021. Construction and Demolition Waste. https://www.recyc-quebec.gouv.qc.ca/sites/default/files/documents/bilan-gmr-2021-crd-english.pdf. Accessed on 1 November 2024.
Sahoo, S.S., Vijay, V.K., Chandra, R., Kumar, H., 2021. Production and characterization of biochar produced from slow pyrolysis of pigeon pea stalk and bamboo. Cleaner engineering and technology 3, 100101.
Sanei, H., Rudra, A., Przyswitt, Z.M.M., Kousted, S., Sindlev, M.B., Zheng, X., Petersen, H.I., 2024. Assessing biochar's permanence: an inertinite benchmark. Int. J. Coal Geol. 281, 104409.
Santos, J.L., Centeno, M.A., Odriozola, J.A., 2023. Biochar production from cellulose under reductant atmosphere: influence of the total pyrolysis time. RSC Adv. 13 (30), 21071–21079.
Sarfaraz, Q., Silva, L.S.D., Drescher, G.L., Zafar, M., Severo, F.F., Kokkonen, A., Solaiman, Z.M., 2020. Characterization and carbon mineralization of biochars produced from different animal manures and plant residues. Sci. Rep. 10 (1), 955.
Sarkar, D., Panicker, T.F., Mishra, R.K., Kini, M.S., 2024. A Comprehensive Review of Production and Characterization of Biochar for Removal of Organic Pollutants from Water and Wastewater. Water-Energy Nexus.
Schorr, D., Boivin, G., 2023. Overview of Canadian CRD Wood Waste Recycling and Valorization Ecosystem. FP Innovations.
Shadangi, K.P., Sarangi, P.K., Behera, A.K., 2023. Characterization techniques of biomass: Physico-chemical, elemental, and biological. In: Bioenergy Engineering. Woodhead Publishing, pp. 51–66.
Sharma, P., 2024. Biochar application for sustainable soil erosion control: a review of current research and future perspectives. Front. Environ. Sci. 12, 1373287.
Spokas, K.A., 2010. Review of the Stability of Biochar in Soils: Predictability of O: C Molar Ratios.
Steven, S., Nugraha, P.Z., Hernowo, P., Oktavia, F.D., Putri, A.H.I., Bindar, Y., 2024. Investigation of high water content in bio-crude oil (BCO) produced from empty oil palm fruit bunches pyrolysis. Biomass Convers. Biorefinery 1–17.
Sun, J., He, F., Pan, Y., Zhang, Z., 2017. Effects of pyrolysis temperature and residence time on physicochemical properties of different biochar types. *Acta Agriculturae Scandinavica, Section B—Soil & Plant*. Science 67 (1), 12–22.
Sun, X., Fu, H., Bao, M., Liu, W., Luo, C., Li, Y., Lu, J., 2022. Development of a new hydrophobic magnetic biochar for removing oil spills on the water surface. Biochar 4 (1), 60.
Tang, E., Liao, W., Thomas, S.C., 2023. Optimizing biochar particle size for plant growth and mitigation of soil salinization. Agronomy 13 (5), 1394.
Tarasov, D., Leitch, M., Fatehi, P., 2018. Lignin–carbohydrate complexes: properties, applications, analyses, and methods of extraction: a review. Biotechnol. Biofuels 11, 1–28.
Tian, Y., Wang, F., Djandja, J.O., Zhang, S.L., Xu, Y.P., Duan, P.G., 2020. Hydrothermal liquefaction of crop straws: effect of feedstock composition. Fuel 265, 116946.
Tomczyk, A., Sokołowska, Z., Boguta, P., 2020. Biochar physicochemical properties: pyrolysis temperature and feedstock kind effects. Rev. Environ. Sci. Biotechnol. 19 (1), 191–215.
Tu, P., Zhang, G., Wei, G., Li, J., Li, Y., Deng, L., Yuan, H., 2022. Influence of pyrolysis temperature on the physicochemical properties of biochars obtained from herbaceous and woody plants. Bioresour. Bioproc. 9 (1), 131.
Usino, D.O., Sar, T., Ylitervo, P., Richards, T., 2023. Effect of acid pretreatment on the primary products of biomass fast pyrolysis. Energies 16 (5), 2377.
Wang, W., Bai, J., Lu, Q., Zhang, G., Wang, D., Jia, J., Yu, L., 2021. Pyrolysis temperature and feedstock alter the functional groups and carbon sequestration potential of Phragmites australis-and Spartina alterniflora-derived biochars. GCB Bioenergy 13 (3), 493–506.
Wang, W., Lemaire, R., Bensakhria, A., Luart, D., 2022. Review on the catalytic effects of alkali and alkaline earth metals (AAEMs) including sodium, potassium, calcium and magnesium on the pyrolysis of lignocellulosic biomass and on the co-pyrolysis of coal with biomass. J. Anal. Appl. Pyrolysis 163, 105479.
Wood, R., Mašek, O., Erastova, V., 2024. Developing a molecular-level understanding of biochar materials using public characterization data. Cell Reports Physical Science 5 (7).
Xiao, X., Chen, Z., Chen, B., 2016. H/C atomic ratio as a smart linkage between pyrolytic temperatures, aromatic clusters and sorption properties of biochars derived from diverse precursory materials. Sci. Rep. 6 (1), 22644.
Xu, C., Wei, K., Du, Z., Ma, W., 2024. Effect of particle size on the properties of biomass gasification residue pellets used as a metallurgical-grade silicon reducing agent. Powder Technol. 435, 119406.
Xu, J., Liu, J., Ling, P., Zhang, X., Xu, K., He, L., Xiang, J., 2020. Raman spectroscopy of biochar from the pyrolysis of three typical Chinese biomasses: a novel method for rapidly evaluating the biochar property. Energy 202, 117644.
Xu, M., Sheng, C., 2012. Influences of the heat-treatment temperature and inorganic matter on combustion characteristics of cornstalk biochars. Energy Fuel 26 (1), 209–218.
Yaashikaa, P.R., Kumar, P.S., Varjani, S., Saravanan, A.J.B.R., 2020. A critical review on the biochar production techniques, characterization, stability and applications for circular bioeconomy. Biotechnology reports 28, e00570.
Yang, K., Huang, J., Dong, B., Liu, P., Chen, L., Wang, Z., Jia, L., 2021. Secondary reactions of primary tar from biomass pyrolysis: characterization of heavy products by FT-ICR MS. Energy Fuel 35 (16), 13191–13199.
Yang, Y., Sun, K., Han, L., Jin, J., Sun, H., Yang, Y., Xing, B., 2018. Effect of minerals on the stability of biochar. Chemosphere 204, 310–317.
Ye, L., Peng, Z., Wang, L., Anzulevich, A., Bychkov, I., Kalganov, D., Jiang, T., 2019. Use of biocarbon for sustainable ferrous metallurgy. Jom 71, 3931–3940.
Zadeh, Z.E., Abdulkhani, A., Aboelazayem, O., Saha, B., 2020. Recent insights into lignocellulosic biomass pyrolysis: a critical review on pretreatment, characterization, and products upgrading. Processes 8 (7), 799.
Zhu, Z., Duan, W., Chang, Z., Du, W., Chen, F., Li, F., Oleszczuk, P., 2023. Stability of functionally modified biochar: the role of surface charges and surface homogeneity. Sustainability 15 (10), 7745.
Zou, X., Debiagi, P., Amjed, M.A., Zhai, M., Faravelli, T., 2024. Impact of high-temperature biomass pyrolysis on biochar formation and composition. J. Anal. Appl. Pyrolysis 179, 106463.